Gaining Microscopic Insight into Molecular Junctions by Transport Experiments

Inauguraldissertation

zur
Erlangung der Würde eines Doktors der Philosophie
vorgelegt der
Philosophisch-Naturwissenschaftlichen Fakultät
der Universität Basel

von

Jan Gerhard Brunner
aus Therwil BL

Basel, 2013

Original document stored on the publication server of the University of Basel
edoc.unibas.ch

This work is licenced under the agreement „Attribution Non-Commercial No Derivatives – 2.5 Switzerland“. The complete text may be viewed here:
creativecommons.org/licenses/by-nc-nd/2.5/ch/deed.en

Genehmigt von der Philosophisch-Naturwissenschaftlichen Fakultät
auf Antrag von
PD Dr. M. Calame
Prof. Dr. C. Schönenberger
Prof. Dr. N. Agraït
Prof. Dr. P. Samorì

Basel, den 18. September 2012

Prof. Dr. Jörg Schibler
Dekan

Contents

1. Molecular Junctions **1**
- 1.1. Molecular Junctions and Molecular Electronics 1
  - 1.1.1. Metal–Metal and Metal–Molecule–Metal Junctions . . . 1
- 1.2. Experimental Technique 4
  - 1.2.1. Fabrication of Lithographically Defined Break Junction Samples 5
- 1.3. Measurements of Pure Solvent and S-OPE-S 5
  - 1.3.1. Data Analysis 7

2. Fluctuations in Molecular Junctions **11**
- 2.1. Experimental methods 11
- 2.2. Identifying random telegraph signals in different molecular solutions 13
- 2.3. Time Development of Lifetimes 14
- 2.4. Automatic measurements with octanedithiol solution 18
- 2.5. Conclusions 20

3. Investigation of Symmetry Aspects by IV Spectroscopy **21**
- 3.1. Development of the IV Measurement Method 21
  - 3.1.1. Determining Operational Parameters for IV Measurements 23
  - 3.1.2. Implementation of a Fast IV Acquisition Setup 25
- 3.2. IV Characteristics of Symmetric and Asymmetric Molecules . . 27
- 3.3. Single Energy Level Model 30
- 3.4. Systematic Investigation of Symmetric and Asymmetric Molecules 33
- 3.5. Development of IV Characteristics on Plateau 36
- 3.6. Conclusions 40

4. The Effect of Polar Anchor Groups **41**
- 4.1. Comparison of Thiol, Isocyanide and Cyanide Linker Groups . 42
- 4.2. Evidence for Molecular Chain Formation in Short Isocyanide Molecules 48
  - 4.2.1. Controlling the Chain Formation 51
- 4.3. Systematic Comparison of Different Diisocyanide Molecules . . 56
- 4.4. Conclusions 58

5. Additional Investigations **61**
5.1. Further Linker Groups 61
5.1.1. Amines 61
5.1.2. Double Thiol Anchor Group 63
5.2. Redox-active Molecules 65

6. Summary and Outlook **69**

A. Investigation of Other Molecules **75**
A.1. Crown Ether molecule 75
A.2. Br-OPE-Br, I-OPE-I 76

B. Specifications of IV converter **79**
B.1. IV Converters 79
B.2. Effects of Large Ramp Speed on IV Converter Gain 79

C. Additional IV Investigations **81**
C.1. Effect of Temperature on Single Energy Level Model 81
C.2. Effect of Bias Range 82
C.3. Unreasonable Fit Parameters 83

D. Supplementary Information for Fluctuations Chapter **85**
D.1. Derivation of the distribution of lifetimes 85

Curriculum Vitae **87**

Publications **89**

Acknowledgements **91**

Chapter 1

Molecular Junctions

1.1. Molecular Junctions and Molecular Electronics

Molecular electronics, the use of the electronic properties of single molecules, has been advertised as a possible successor of CMOS technology. Applications for computing seem very unlikely for fundamental reasons. The tradeoff between function, which need well-defined energy levels, and good transport for fast processing which broadens the energy levels is one example. Another reason is the difficulty of contacting single molecules in a confined space. Still, the field is very interesting for basic research as fundamental properties of molecules and molecule–metal bonds are investigated on a single molecular level. Related fields like organic electronics have already spawned applications, the most prominent of which are organic light emitting diodes (OLEDs) which are being used as light sources and in displays. Such applications might profit from knowledge gained from single molecule experiments where, for example, the coupling of molecules to metal electrodes can be studied on a more fundamental level than in large systems.

In this work, an introduction to molecular junctions is given in chapter 1. Conductance fluctuations of molecular junctions are studied to learn about the stability of molecule–gold bonds (chapter 2). The knowledge about the instability of molecular junctions is then applied to develop an efficient method of measuring current–voltage characteristics of single molecules (chapter 3). This method is used to compare the effect of different linker groups on coupling constants and energy level alignment. Isocyanide is investigated as linker group and compared to cyanide and thiol in chapter 4. It exhibits interesting properties that are not observed for most other linker groups. Additional investigations that are not part of the main projects are presented in chapter 5 and in appendix A.

1.1.1. Metal–Metal and Metal–Molecule–Metal Junctions

It has been known for some time that thin wires of gold or other metals can form monoatomic constrictions or even chains when they are stretched [1–3].

The formation of chains not more than one gold atom wide was indirectly demonstrated at first by observing the theoretically predicted lowest ballistic conductance value of $1\,G_0 = 2e^2/h = (12.9\,\mathrm{k\Omega})^{-1}$ during the breaking process of gold wires [1]. Shortly after, atomic gold chains were actually imaged by transmission electron microscopy while simultaneously measuring the corresponding conductance values [4]. The most common experimental techniques to create monoatomic contacts employ either a scanning tunnelling microscope (STM) or a mechanically controllable break junction (MCBJ).

The small electrode tips created by breaking thin metal wires can be used to contact single molecules. In most cases, molecules with two binding groups with a high affinity to gold are used [5]. The molecules can then bind to both electrodes forming a metal–molecule–metal junction. In the following section, the MCBJ technique used in this work is described. Table 1.1 lists the molecules investigated in this work and their source. All molecules were used as received with no further purification steps.

Molecule	Source	synthesised by	Chapters
S-OPE-S	Group of M. Mayor, University of Basel	S. Grunder	1, 3
N-OPE-N	Group of M. Mayor, University of Basel	S. Grunder	3
N-OPE-S	Group of M. Mayor, University of Basel	S. Grunder	3
1-NC	Group of M. Mayor, University of Basel	M. Gantenbein	4
2-NC	Group of M. Mayor, University of Basel	M. Gantenbein	4
3-NC	Group of M. Mayor, University of Basel	M. Gantenbein	4
1-mNC	Group of M. Mayor, University of Basel	M. Gantenbein	4
3-CN	Group of M. Mayor, University of Basel	D. Vonlanthen	4
3-SAc	Group of M. Mayor, University of Basel	D. Vonlanthen	4
OPE diamine	Group of M. Mayor, University of Basel	N. Jenny	5
SS-OPE-SS	Group of M. Mayor, University of Basel	M. Bohrer	5
OPVFccenter	Group of M. Mayor, University of Basel	S. Grunder	5
OPVFcside	Group of M. Mayor, University of Basel	N. Jenny	5
OPVFccontrol	Group of M. Mayor, University of Basel	N. Jenny	5
crown ether	Group of M. Mayor, University of Basel	D. Vonlanthen	A
Br-OPE-Br	Group of M. Mayor, University of Basel	N. Jenny	A
I-OPE-I	Group of M. Mayor, University of Basel	N. Jenny	A
hexanedithiol	Sigma-Aldrich	commercial	2
octanedithiol	Sigma-Aldrich	commercial	2
nonanedithiol	Sigma-Aldrich	commercial	2
diaminooctane	Sigma-Aldrich	commercial	5

Table 1.1.: Table of the molecules used in this work and their sources.

1.2. Experimental Technique

Mechanically controllable break junctions (MCBJ) consist of free-standing conductive leads on a flexible and non-conductive or insulated substrate. Figure 1.1a shows the setup used in this work and the electronic circuit is shown in figure 1.1b. A liquid cell is attached on top of the break junction sample to allow for measurements in liquid environments. The connection between the sample and the liquid cell is sealed by a flexible Viton O-ring to accommodate for the bent sample. The sample is bent by moving up a push rod (Δz). This stretches the free-standing gold bridge which eventually breaks, forming two gold electrodes. Their separation d now linearly depends on the push rod position z with an estimated attenuation factor $a = \Delta d/\Delta z$ in-between $1.5 \cdot 10^{-5}$ and $4 \cdot 10^{-5}$ [5]. This low attenuation factor allows for a fine adjustment of the electrode separation and leads to a low sensitivity to vibrations. The current is measured with an auto ranging I to V converter with four gain settings from 10^4 to 10^9 V/A (SP895c/d, University of Basel) or from 10^5 to 10^8 V/A (SP895/SP895a, University of Basel). Normal open/close cycles are performed as follows. A fixed low bias voltage of typically 0.1 or 0.2 V is applied to the break junction with a series resistor of 1 kΩ to protect the sample from large currents at high conductance values. The push rod is now moved up at a speed of typically 31.2 µm/s the conductance reaches the background noise level of the setup of about $10^{-6}\,G_0$ plus an additional 50 µm. The push rod is then moved back down until the conductance reaches a threshold of typically $10\,G_0$. This open/close cycle repeats until enough data has been collected or the life time of the sample has ended.

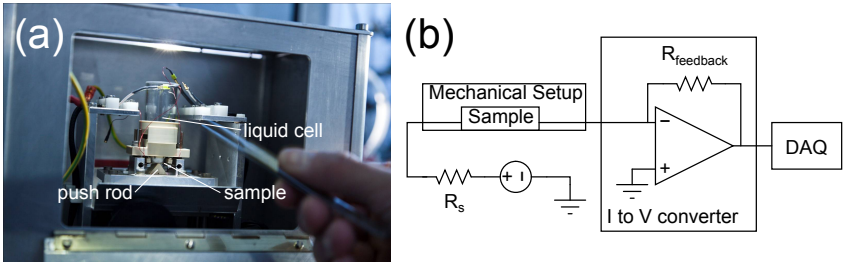

Figure 1.1.: (a) Photograph of the MCBJ setup used in this work. Sample, push rod and liquid cell are indicated. The experimenter's hand is shown for scale. (Photograph by courtesy of Stefano Schröter). (b) Schematic of the electronic setup. A voltage source is connected to one contact of a break junction. The other contact is connected to the input of an I/V converter. The output voltage of the I/V converter is measured by a data acquisition board (DAQ) and recorded on a computer.

1.2.1. Fabrication of Lithographically Defined Break Junction Samples

The break junction samples used in this work were prepared as follows. Spring steel with a thickness of 0.3 mm was covered by a polyimide insulation layer of a few µm. Gold leads with two individually addressable constrictions were prepared by electron beam lithography and physical vapour deposition (10 nm Ti + 60 nm Au). The titanium adhesion layer was evaporated at an angle of 47° from perpendicular in order to obtain a pure gold wire at the constriction. An additional insulation layer of photodefinable polyimide was added on top of the gold traces in order to lower the leakage current when measuring in ionic environments. In those protected samples the gold traces are only exposed to the solution over a distance of 10 µm. Before measuring, the polyimide was dry etched in an O_2/CHF_3 plasma in order to expose free-standing gold bridges. Figure 1.2 shows typical break junction samples after etching. The two free-standing gold bridges and the 10 µm gap in the polyimide top insulation layer is visible.

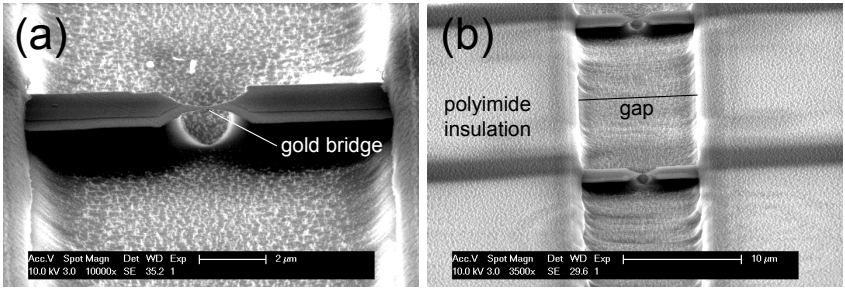

Figure 1.2.: SEM images of typical break junction samples showing the free-standing gold bridges and the 10 µm wide gap in the polyimide insulation layer.

1.3. Measurements of Pure Solvent and S-OPE-S

Oligo (phenylene ethynylene) (OPE) is a well-studied molecule for molecular electronics experiments [6, 7]. In this section, a version with two acetyl-protected thiol linker groups, S-OPE-S, will be measured with the MCBJ setup and compared to data obtained in pure solvent. The chemical structure of S-OPE-S is shown at the top of figure 1.3.

As solvent, a mixture of tetrahydrofuran (THF) and mesitylene in a ratio 1:4 was employed. THF is polar which is needed in order to dissolve S-OPE-S and many other molecules. But pure THF is also quite volatile and will soften

and swell the Viton O-ring between sample and liquid cell. Mesitylene is non-polar, less volatile and will not harm the O-ring. The mixture is therefore a compromise between the properties of both solvents. S-OPE-S was dissolved in THF/mesitylene 1:4 to form a solution with a concentration of 0.2 mM. In order for S-OPE-S to form covalent bonds to the gold electrodes, the acetyl protection groups have to be removed from its thiol end groups. This is accomplished by adding tetrabutylammonium hydroxide (TBAH) at a concentration of 0.05 mM. Argon is bubbled through the solution to purge oxygen throughout the measurement. This is necessary to prevent the polymerisation of S-OPE-S by disulphide bond formation.

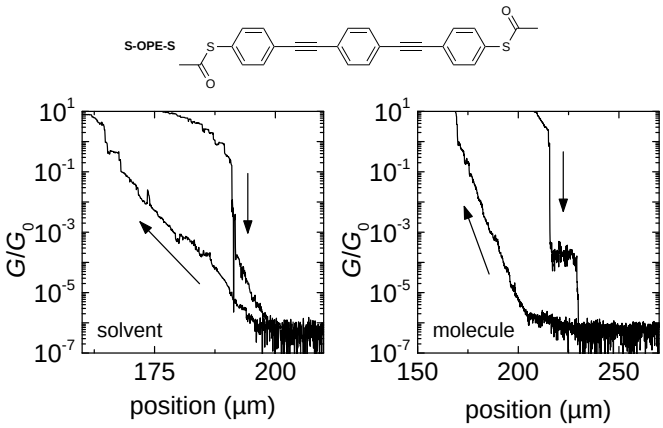

Figure 1.3.: Typical opening and closing curve for pure solvent (THF/mesitylene 1:4) and a molecular solution of 0.2 mM S-OPE-S in THF/mesitylene 1:4. The closing curve (up arrow) was recorded right after the opening curve (down arrow) in both cases.

Figure 1.3 shows a typical opening and closing curve measured in pure solvent (left) and in the S-OPE-S solution (right). In the opening curves (down arrow), the conductance of the junction is steadily decreasing at first as the gold bridge is becoming narrower. At lower conductance values, the junction starts to behave ballistically, preferentially taking conductance values close to integer multiples of the quantum of conductance G_0 decreasing in steps down to $1\,G_0$ where the junction is just one gold atom wide [1]. With further opening, the gold bridge breaks and the electrodes quickly separate by a few Å due to mechanical relaxation. In pure solvent, this causes the conductance to jump down to between 10^{-2} and $10^{-4}\,G_0$ and electron transport is now provided by tunnelling. Further opening of the junction leads to an exponential decrease of the tunnelling conductance ($G \propto \exp(-\beta d)$) until the detection limit is

reached at about $10^{-6}\,G_0$ (depending on the bias voltage, the noise level of the environment, the sample and the measured solution). If the opening is performed in a solution of S-OPE-S, the exponential decrease of the conductance or even the quick decrease after breaking can be interrupted by a molecule bridging the gap between the electrodes. This leads to the formation of a conductance plateau as seen in figure 1.3 the example at about $2 \cdot 10^{-4}\,G_0$. During the conductance plateau, the molecule is either sliding on the gold electrodes to accommodate further electrode separation or the molecule and its bonds to the gold tips are stretched if it is already connected at the very end of the electrodes. At the low stretching speed in our setup of typically $\approx 1\,\mathrm{nm/s}$, the molecule–metal bonds break spontaneously in most of the cases with forces below the maximum forces sustainable by the bond [8, 9]. When closing the junction, an exponential increase of the conductance is observed both without and with molecules.

1.3.1. Data Analysis

The conductance traces differ from each other due to random influences such as exact atomic positions and thermal motion. It is therefore necessary to statistically analyse many conductance traces in order to obtain reproducible conductance values. Because the conductance traces range over several orders of magnitude and contain an exponential tunnelling decay, it is convenient perform statistics in a logarithmic scale [5]. Figure 1.4 shows logarithmic histograms of opening curves in pure solvent (green) and in the S-OPE-S solution (red). Both histograms show a peak at $1\,G_0$, corresponding to the monoatomic gold contact before breaking. The quick conductance decrease due to mechanical relaxation leads to a range of low counts between $1\,G_0$ and $10^{-3}\,G_0$. In the solvent case, the exponential decrease due to tunnelling translates to a flat region between 10^{-4} and $10^{-6}\,G_0$. In the case of S-OPE-S solution, the molecular plateaus translate to a histogram peak. A Gaussian fit to this peak leads to a conductance value of $2.3 \cdot 10^{-4}\,G_0$ (most likely value in the logarithmic representation).

2D histograms are an alternative way to display opening or closing conductance data from break junction measurements. Hereby, the individual curves are shifted to coincide at a defined conductance value. A 2D density map is then generated from all the curves. Figure 1.5 shows typical curves and corresponding 2D histograms of both opening (a) and closing (b) in THF/mesitylene 1:4. For the opening data, the curves were overlapped at $G = 0.5\,G_0$ whereas $G = 10^{-5}\,G_0$ was chosen for the closing curves. This representation has the advantage of retaining position-dependent information. In addition, outlier curves in which the conductance is changing very slowly with respect to the position for unwanted (nano)mechanical reasons have little effect on the overall look of the 2D histograms whereas such curves have to be rejected for 1D histograms

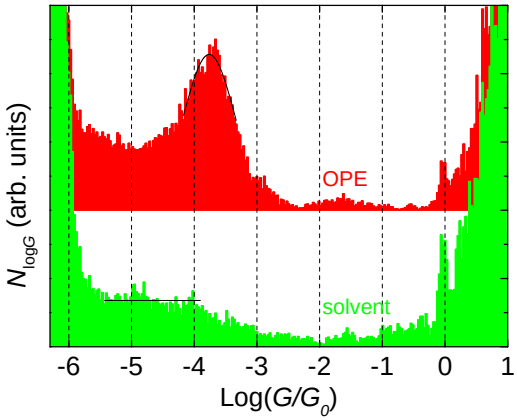

Figure 1.4.: Conductance histograms of 78 consecutive opening curves for pure solvent (green) and 86 consecutive opening curves of S-OPE-S solution (red).

due to their big influence on the statistics which can lead to false conductance peaks. The exponential decrease as well as the increase in conductance in the opening and closing curves, respectively, translates to a high density along an approximately straight line in the 2D histograms as indicated by red lines.

Data measured in S-OPE-S solution is shown in figure 1.6. Well-defined plateaus are observed in about 70% of the opening curves around $G_1 = 2.3 \cdot 10^{-4}\, G_0$ (a). This translates to a high density in the 2D histogram around G_1. Most of the closing curves (b) show an exponential increase in conductance. Conductance jumps are rarely observed in approximately 5% of the closing traces. Two examples of such jumps are shown on the left (first and third curve from the right). The conductance values right after the jumps are in approximate agreement to the molecular conductance value G_1 obtained from opening curves. Such jumps to contact have been proposed as an alternate method to obtain single-molecular conductance [10, 11]. In the present data, the jumps are too rare to show up in the 2D histogram where mostly an exponential increase in tunnelling conductance is observed as in the pure solvent case. S-OPE-S and other variants of OPE will be studied in more detail in chapter 3.

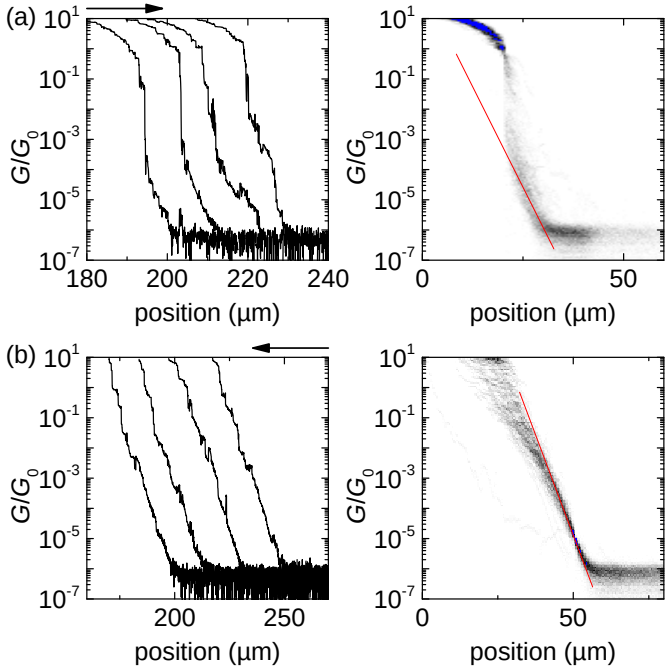

Figure 1.5.: (a) Typical opening curves in THF/mesitylene 1:4 (left) and a 2D histogram of 99 consecutive opening curves (right). After a fast breaking to $\approx 10^{-3}\,G_0$ an approximately exponential decrease in conductance is observed. (b) Typical closing curves of THF/mesitylene 1:4 (left) and a 2D histogram of 99 consecutive closing curves aligned at $10^{-5}\,G_0$ (right). A clean exponential increase in conductance is observed. The red lines indicate an exponential decay with the same decay constant in both (a) and (b).

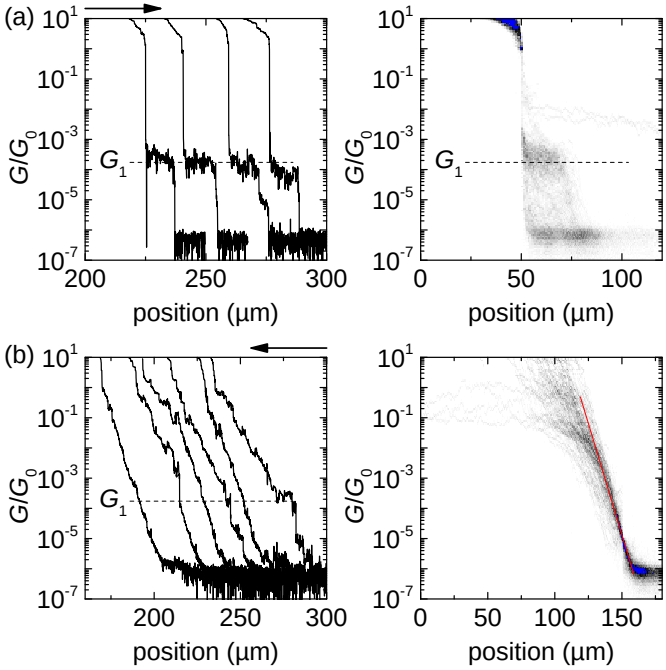

Figure 1.6.: (a) Typical opening curves with plateau of 0.2 mM OPE disulphide in THF/mesitylene 1:4 (left) and a 2D histogram of 143 consecutive opening curves (right). Plateaus are observed around $2.3 \cdot 10^{-4}\, G_0$ in about 70% of the curves. (b) Typical closing curves of OPE disulphide (left) and a 2D histogram of 143 consecutive closing curves aligned at $10^{-5}\, G_0$ (right). Jumps to molecular contacts are observed in about 5% of the curves. On average, an exponential increase of the conductance with decreasing distance is observed as indicated by the red line.

Chapter 2

Fluctuations in Molecular Junctions

Reliable contacts are a requirement for future applications of single molecular electronics. Studies have been made on the mechanical and thermodynamic stability of the common sulphur–gold bonds [8, 12, 13] but the dynamic properties of metal–molecule–metal contacts are still unclear. Our way of investigating the dynamics of molecular junctions is to analyse the conductance signal in a mechanically controllable break junction setup. Specifically, the conductance fluctuations observed in break junctions immersed in a solvent with and without alkanedithiols are investigated in this chapter. The fluctuations are recorded for successive fixed gold electrodes separations. In the presence of alkanedithiols, random telegraph signals (RTS) are clearly observed which are attributed to the repeated formation and breaking of molecule - gold bonds. We find that these signals can show different relative amplitudes with state lifetimes ranging between 0.1 ms and 0.1 s. This is in agreement with observations in STM break junction measurements. We also show that for measurements in pure solvents, RTS are much rarer while the amplitude of the conductance fluctuations remain substantially smaller.

2.1. Experimental methods

The measurements were performed with a mechanically controlled break junction setup as illustrated in figure 2.1a. The samples are produced as demonstrated in section 1.2.1.

During measurements, the break junctions are immersed in a liquid environment consisting of either pure mesitylene or solutions of 1 mM alkanedithiols in mesitylene. A constant bias voltage of 0.2 V is applied in order to determine the conductance $G(t)$. The current is measured by an auto-ranging current to voltage converter with a gain range from 10^4 to 10^9 V/A. This allows the

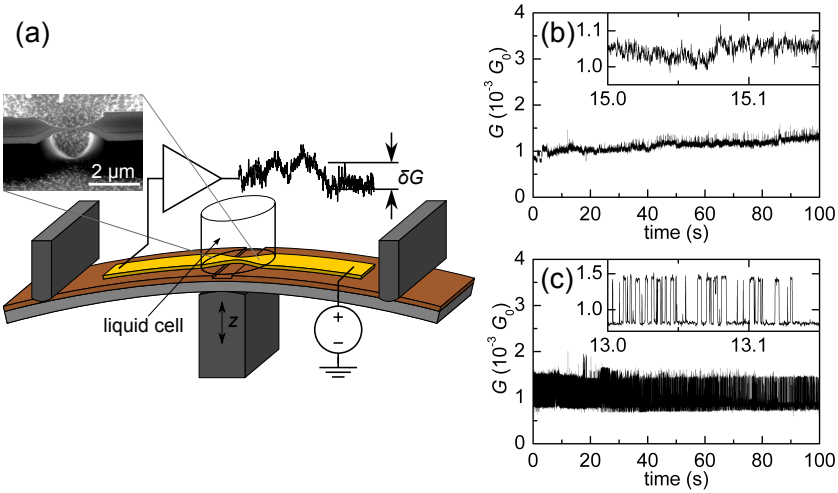

Figure 2.1.: (a) Sketch of the MCBJ setup: A free-standing bridge is situated inside a liquid environment. The bridge can be broken and re-closed by moving the push rod up and down. The conductance is obtained by applying a bias voltage to the gold bridge and measuring the current with an auto-ranging I-V converter. Typical $G(t)$ trace observed in pure solvent (mesitylene) (b) and a trace showing a random telegraph signal measured in hexanedithiol solution (c).

measurement of conductance over many orders of magnitude from mechanically closed contacts ($G > 10\,G_0$, $G_0 = 2e^2/h$) down to large tunnelling gaps ($G \approx 10^{-7}\,G_0$). The upper frequency limit of the amplifier is approximately 1.3 kHz at the highest gain setting and 10 kHz at the lower gains.

All measurements were started with the junction completely open (conductance below the detection limit). Two different types of measurements are then performed from this state. In the manual measurements, the push rod is gradually moved while observing the conductance at a low sampling rate. When signals of interest (large fluctuations) are observed, the movement is stopped and 100 s intervals are recorded at a sampling rate of 10 kHz. For the systematic measurements, the junction is automatically closed to $10^{-5}\,G_0$ and further closed in small steps ($\Delta d \approx 0.1$ Å) once every 30 s. The conductance is recorded at a sampling rate of 50 Hz in this case. The electrodes are not actively moved during conductance measurements. We anticipate that the gold surfaces have time to relax and we expect no force to be acting on the tips.

2.2. Identifying random telegraph signals in different molecular solutions

The manual measurement method was used to closely analyse the observed signals. Figure 2.1 shows signals measured in both pure solvent and a solution of gold-binding molecules. When the break junction is surrounded by pure mesitylene (figure 2.1b), the conductance signal mostly consists of random fluctuations. Note that there is a small drift in this measurement which we attribute to the deformation of either the adhesive tape employed to prevent shorts between the counter supports and the substrate or parts of the mechanical setup. In most measurements, the observed drift is small and can be neglected (figure 2.5). When the measurement is done in a hexanedithiol solution, stronger fluctuations are sometimes observed as shown in figure 2.1c. In this particular time interval, the conductance shows switching between two well-defined values for most of the time. The conductance stays at one value before suddenly switching to the other value at a random point in time. The time scale of the actual switching event could not be resolved by our setup. Such signals are called two-level random telegraph signals (RTS) and they are analysed in more detail in the following paragraphs.

A common way to identify and analyse RTS is to look at frequency spectra [14–17]. From theory, we expect the spectrum of an RTS to be of a Lorentzian shape. Figure 2.2b shows the frequency spectra of the two marked time intervals in a measurement of nonanedithiol solution shown in figure 2.2a. Indeed, we observe a Lorentzian spectrum during an interval with clear RTS (1), in agreement with theory [18], whereas the non-RTS part (2) results in a $1/f$ spectrum. The grey area indicates the region above the cutoff frequency of the amplifier at $\approx 1.3\,\mathrm{kHz}$.

Figure 2.2c shows a section of the same measurement obtained in a nonanedithiol solution where a clear RTS is observed. The state lifetimes are obtained from the conductance trace as indicated in the figure for the high conductance states. Three reference levels (shown as horizontal dashed lines) are defined to be typically at 10, 50 and 90% of the range between the low and high conductance values. The time interval between a mid reference level crossing and the closest following one that occurs after at least one crossing of a high (low) reference level corresponds to a high-state (low-state) lifetime. A histogram of these state lifetimes $t_{\mathrm{h},i}$ is shown in figure 2.2d. This method is only valid if the amplitude of the background noise is much lower than the RTS amplitude which is fulfilled in this example.

The histogram shown in figure 2.2d shows a fast decay. Fitting an exponential decay function $\propto e^{-t/\tau}$ (dashed red curve) to the histogram yields the average lifetime $\tau_{\mathrm{high}} = 1.9\,\mathrm{ms}$ of the corresponding state ($\tau_{\mathrm{low}} = 0.93\,\mathrm{ms}$). For most observed RTS, the fit is significantly more accurate when using a sum of two

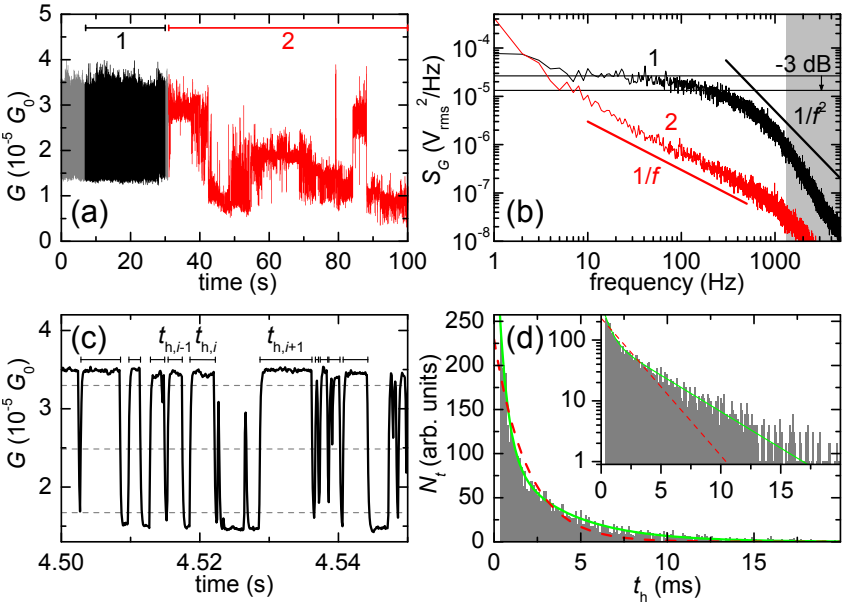

Figure 2.2.: (a) Complete $G(t)$ trace measured in nonanedithiol solution showing RTS during the first 30 s, then random fluctuations. (b) Power spectra of the corresponding intervals shown in (a). (c) Section of a random telegraph signal measured in nonanedithiol solution with high conductance state lifetimes marked. (d) Histogram of the lifetimes with exponential decay fits to obtain the average lifetime. Single exp (dashed red) and sum of two exp (solid green). Inset: Same data in logarithmic scale.

exponential decays (solid green curve) or a stretched exponential. Using more than two exponential functions provides no substantial further improvements. Plotting the state lifetimes and a sliding average of the values shows that the average lifetimes change on a time scale of several seconds (see figure 2.3). In a few cases, the average lifetimes stay approximately constant (figure 2.4) and a single exponential accurately fits the lifetime distribution.

2.3. Time Development of Lifetimes

Such fits were done on the data of 16 measurement sets from 12 samples. The lifetimes obtained from these fits vary between ≈ 1 and 100 ms where the lower limit is set by the bandwidth of the amplifier. We did not observe a difference between the high and the low conductance state lifetimes and the lifetimes do not depend on the length of the alkyl chains.

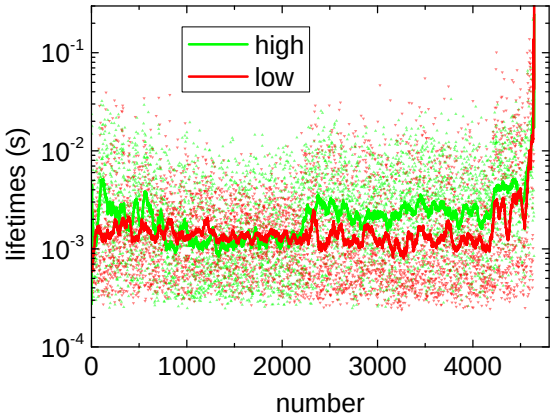

Figure 2.3.: Scatter plot of the lifetimes obtained from the nonanedithiol measurement shown in figure 2.2. The high and low state lifetimes are shown in green and red, respectively. The lines are logarithmically averaged values over windows of 50 events. A clear change of the average high conductance state lifetime is seen, for example, at event number 2200.

In the following discussion, we try to deduce the microscopic origin of the observed RTS. The two conductance values observed in an RTS must correspond to at least two states of the junction. Different mechanisms causing the conductance change can be envisioned as the changes could involve the contact between the molecule and the gold electrodes, the electrodes alone, the environment of the junction or the molecular structure.

The easiest two imaginable states are one molecule being either bound to both electrodes or to just one electrode with the other bond temporarily broken. Transport through the molecular structure, even if it does not contain delocalised electrons, is usually significantly more efficient than direct tunnelling through vacuum or solvent for the molecular lengths investigated in this work [19]. We would therefore expect a strong difference in the conductance between those two states even if the distance between the electrodes remains the same.

A distance change between the electrodes caused by thermal fluctuations is a probable explanation for fluctuations and even low-amplitude RTS (figure 2.5a) observed in pure solvent. When we assume a constant tunnelling decay constant $\beta \approx 1\,\text{Å}^{-1}$ [20], typical conductance fluctuations with $G_\text{h}/G_\text{l} \approx 1.25$ would correspond to a distance change of $\approx 0.22\,\text{Å}$ which is plausible to happen at room temperature. We assume $G \propto \exp(-\beta/d)$. This means that $G_\text{h}/G_\text{l} =$

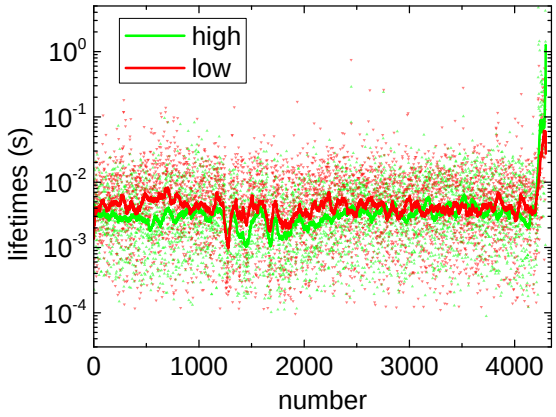

Figure 2.4.: Scatter plot of the lifetimes of a hexanedithiol measurement which shows no clear changes of the average state lifetimes. A single exponential decay fits well to the lifetime distribution.

$\exp(-\beta(d_\mathrm{h} - d_\mathrm{l}))$ and therefore $\Delta d = d_\mathrm{l} - d_\mathrm{h} = -\ln(G_\mathrm{h}/G_\mathrm{l})/\beta$. Note that thermal fluctuations occur at a much faster time scale than the bandwidth of our setup. This means that we cannot observe the full fluctuation amplitude and the distance fluctuation is estimated as a lower limit of the true movement. We cannot apply the same explanation for the large-amplitude RTS observed with alkanedithiols. Strong conductance fluctuations as those observed with $G_\mathrm{h}/G_\mathrm{l} \approx 3$ would correspond to a distance change of ≈ 1.1 Å which is improbable to repeatedly happen at room temperature.

The environment was shown to have little effect on the conductance of molecular junctions [11] except in special cases [21], so it is probably not the cause of the observed RTS. However, changes in the environment could affect the lifetimes of the RTS states or cause the RTS to end due to steric hindrance. Another possibility is linked to the flexibility of alkane chains. They can change their conformation, e.g. from all-trans to one gauche defect, which would lower the conductance by approximately a factor 10 [22, 23] or even more [24] but the conformations are expected to change at a time scale of 10^{-11} to 10^{-9} s so averaged values would be observed in our measurements [22, 24]. Finally, a sulphur–gold bond could switch between atop and bridge arrangement, leading to a conductance change by a factor of approximately 2 for one contact [22–24].

Considering all mentioned explanations for RTS, a molecule – metal bond

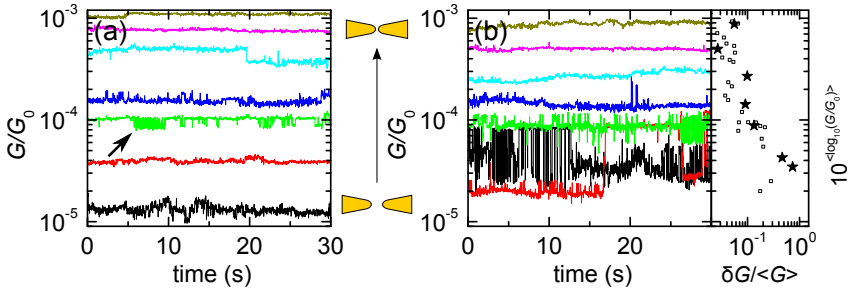

Figure 2.5.: (a) and (b) Typical $G(t)$ traces without and with octanedithiol, respectively. The push rod was not moved during the 30 s traces. In pure solvent (a), conductance fluctuations of mostly small amplitudes are observed. There were occurrences of RTS of small amplitude and short duration (arrow). In the dithiol containing solution (b), conductance fluctuations and sometimes RTS of larger amplitude were observed. The open squares on the right show the relative fluctuation amplitudes for each 30 s interval of one closing/stopping ramp against the logarithmic average of its conductance. The stars indicate the values for the typical curves shown.

repeatedly forming and breaking seems the most probable one. In that case, we would expect a thermally activated forming and breaking of the bond which would lead to exponentially distributed low and high conductance lifetimes. In the following we discuss the lifetime distributions in more detail.

A theoretical two-state random telegraph signal always takes one of two defined values as in the observed cases. While the signal is in one conductance state, there is a constant probability density $1/\tau$ for it to switch to the other state. This leads to the lifetimes of each state to be exponentially distributed with the average lifetime τ (see section D.1).

The fact that the sum of two exponential decays usually provides a better fit could mean that the average lifetimes vary during the measurement time. We can imagine two different ways for this to happen. First, there could be more than two microscopic states that are reached during an RTS. Some of those states could have similar conductance values but different lifetimes. Second, there could be exactly two reachable states for one time interval but their energies and lifetimes could change over time because of changes in the environment. The second explanation is the more likely one, since the time development of the lifetimes shows sudden changes of the average lifetimes with the changes happening at a much slower time scale (figure 2.3). A stretched exponential is empirically fitting to the lifetime distributions for some measurements but it would require a broad distribution of the average lifetimes [25] which is not compatible with the observed rare changes of the average lifetimes.

The observed range of lifetimes in RTS is comparable to the lifetimes of

molecular junctions measured in a liquid environment with an STM when retracting the tip at low velocity [8] which suggests that the RTS lifetimes are also caused by a molecular junction forming and breaking. Indeed, similar conductance fluctuations were observed in the same work during slow opening cycles. Note that much longer lifetimes of molecular junctions have been observed in vacuum [12] where the mobility of the molecules is lower.

From the RTS observed, we notice no dependence of τ_h and τ_l on the conductance. This suggests that the different lifetimes are caused by different microscopic arrangements of gold atoms and molecules as opposed to a smaller gap being energetically more favourable to be bridged by a molecule than a larger one.

Both the absolute and relative conductance values of the RTS states and their lifetimes vary considerably in our measurements. If they are to be used as fingerprints specific to a molecule, care has to be taken to provide conditions where reproducible values can be obtained.

Clear RTS were a rare occurrence ($\approx 1\%$ of the time) which prevented a statistical investigation of their properties as done in other systems [26]. Similar RTS were also observed in solutions of OPE with thiol linker groups. OPE has a rigid backbone so in this case, gauche/trans transitions can definitely be ruled out as possible source of conductance fluctuations.

2.4. Automatic measurements with octanedithiol solution

Automatic measurements were employed to obtain an overview of possible fluctuation amplitudes in the investigated junctions.

We have shown typical $G(t)$ traces in figure 2.5a and 2.5b in a logarithmic scale that were automatically recorded in mesitylene without and with octanedithiol, respectively. The G traces in pure mesitylene show conductance fluctuations and sometimes jumps of small relative amplitude. RTS are rare and of short duration and low amplitude (arrow). The relative conductance fluctuation amplitude $\delta G_\mathrm{rel} = \delta G / \langle G \rangle$ (standard deviation of G divided by average of G) does not show any dependence on conductance. With an octanedithiol solution, fluctuations of much higher amplitude are observed at low conductance, between $10^{-5}\,G_0$ and $10^{-4}\,G_0$.

To quantify the fluctuation amplitudes, δG_rel was calculated for each 30 s interval (shown for one octanedithiol measurement on the right of figure 2.5b). The resulting values for one measurement in pure mesitylene (a) and octanedithiol solution (b) are plotted as coloured symbols in figure 2.6. Points shown by one symbol in the same plot represent consecutive conductance traces recorded with a gradually lowered push rod (closing the junction). The outlined histograms on top show the distribution of the average conductance values while closing.

The filled histograms were obtained from opening cycles and are shown for comparison. On the right of the scatter plots, outlined histograms show the distribution of fluctuation amplitudes.

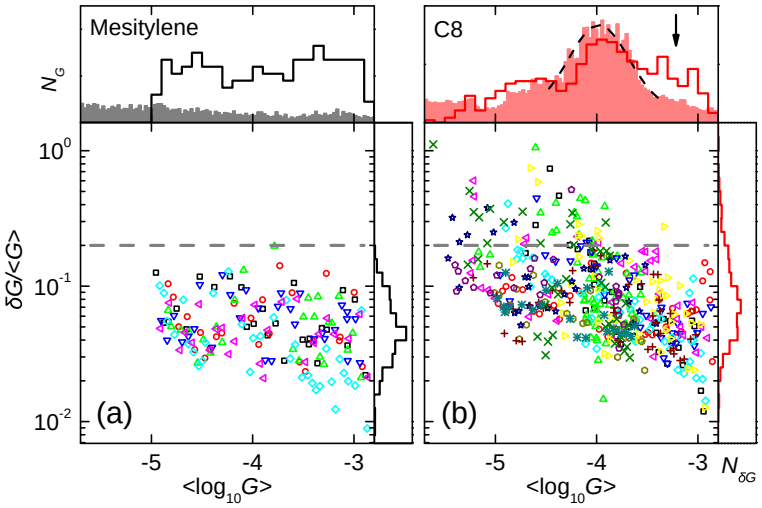

Figure 2.6.: Bottom: The standard deviations of the conductance during 30 s intervals divided by the average conductance of the interval. Plot (a) is obtained from a measurement in pure mesitylene whereas for (b) a solution of octanedithiol in mesitylene was used. The dashed grey lines serve as guides to the eye and indicate the maximum fluctuation amplitude in the pure solvent case. Top: Typical histograms from opening $G(z)$ curves in mesitylene and octanedithiol solution (filled) and conductance histograms of the data below (outlined). The dashed black curve indicates a Gaussian fit to the octanedithiol histogram as a guide to the eye. Histograms of the $dG/\langle G\rangle$ data are shown to the right of the corresponding data. The histograms are normalised to the number of curves or data points for opening curves and closing steps, respectively.

The δG_{rel} values are spread over one order of magnitude with pure mesitylene and decrease only slightly with increasing $\langle G\rangle$. With octanedithiol solution, fluctuations of higher amplitude are present for $\langle G\rangle$ up to the known molecular conductance for octanedithiol.

The conductance histogram of the closing ramp shows a large number of counts between 10^{-4} and $10^{-3}\,G_0$ (indicated by the arrow) as compared to the typical Gaussian distribution in opening cycles (dashed line). This can be explained by two related mechanisms: First, the slow closing of the electrodes

allows for Au relaxation of the electrode apexes leading to a larger surface and thereby more molecules in parallel [27]. Second, layers of molecules formed on the electrodes will impede further closing of the electrodes below a separation distance on the order of one molecular length causing a plastic deformation of the gold. This will lead to both more histogram counts in the associated conductance regime and to even blunter tips than by Au relaxation alone.

The automatic measurements show that while low-amplitude fluctuations are present in measurements with pure solvents as well as in octanedithiol solution, the large-amplitude fluctuations are caused by the gold-binding molecules. The amplitudes of the large conductance fluctuations are on the order of single-molecular conductance values. This explains why the fluctuations are not visible anymore in conductance ranges well above the single-molecular conductance. Even if single molecules bind and unbind at those conductance values, averaging would hide the associated conductance fluctuations.

2.5. Conclusions

RTS are sometimes observed during break junction experiments in a solution of gold-binding molecules. They are most probably caused by molecules spontaneously binding and unbinding to the two electrode tips, thereby forming or breaking a metal–molecule–metal junction. Both the formation and the breaking of the molecule–metal bonds are thermally activated which shows in an exponential distribution of the lifetimes of the conductance states.

We think that the observed fluctuations are a direct evidence that we are dealing with single or few molecular junctions. The varying RTS amplitudes and time scales reflect the different microscopy arrangements and conductance values possible in such experiments. From the observed time scales it can be concluded that in order to reliably obtain properties of a single molecular junction, the time resolution should be as high as possible. In the following chapter, this knowledge will be applied to the measurement of current–voltage characteristics.

Chapter 3

Investigation of Symmetry Aspects by IV Spectroscopy

The constant bias break junction technique discussed in the previous chapters (sections 1.2, 1.3 and 2) provide some insight into the formation of molecular junctions and their stability. However, the knowledge gained about the transport properties of the junction is very limited in those measurements (ohmic resistance). It is therefore of great interest to obtain non-linear current–voltage (IV) characteristics of molecular junctions. Such data would allow, for example, to learn about the electronic structure of molecules and energy level alignment or directly observe diode-like behaviour. In this chapter, a method for measuring IV curves in a break junction setup is presented and employed to measure both symmetric and asymmetric OPE molecules. A simple analytical model is then used in order to extract physical parameters from the IV data.

3.1. Development of the IV Measurement Method

There are several requirements to measure IV curves of molecular junctions in solution. An important one is that any leakage current added to the molecular and tunnelling current measured at the drain side of the junction is significantly lower than the current through the molecule. The main contribution to this undesired current flows from the source electrode through the solution to the drain electrode. It is critically high mostly when there are ions in the solution as, for example, tetrabutylammonium hydroxide (TBAH) which is used to remove the acetyl protection group from thiol linkers. The magnitude of the leakage current can be greatly reduced by decreasing the surface area of the contact leads which is exposed to the solution. Applying a polyimide layer on top of the gold leads except for a small area around the actual junctions as shown in section 1.2.1 is a straightforward way of accomplishing that requirement. In

addition, the width of the gold leads in the uncovered area was reduced. The effect of those measures is shown in the following paragraph.

Figures 3.1 and 3.2 show the leakage current of a fully opened junction in TBAH/mesitylene 1:4 without and with TBAH while sweeping the bias voltage downwards at a rate of 2 V/s. The dashed line indicates the expected current from an idealized ohmic conductance of $10^{-5}\,G_0$ which is about the lowest conductance expected from the molecules to be investigated [6, 7, 28]. The leakage current of pure solvent without TBAH is negligible both with and without the polyimide insulation (figure 3.1). The polyimide layer is absolutely necessary, though, for typical TBAH concentrations (figure 3.2) as the leakage current would otherwise dominate the molecular current. By changing from the normal sample to the new, covered sample, the leakage current is reduced by a factor of 3000 and is now well below the lowest expected molecular currents in the tested voltage range of ±2.0 V.

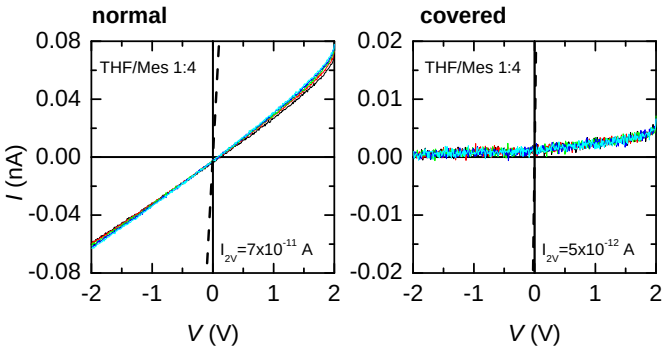

Figure 3.1.: Comparison of the leakage currents in pure solvent (THF/mesitylene 1:4). Left: Normal sample without additional insulation. Right: New sample type with thin leads and polyimide insulation. The dashed line shows the current expected from a $10^{-5}\,G_0$ linear conductance.

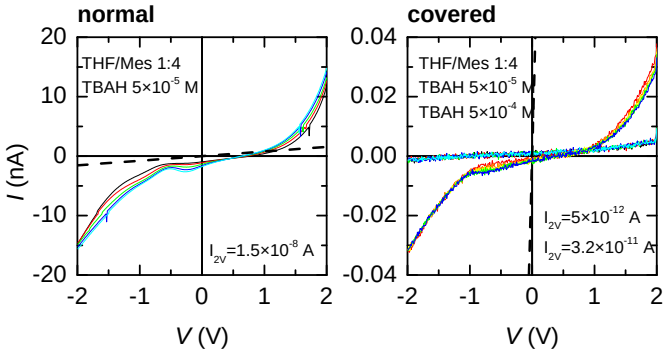

Figure 3.2.: Comparison of the leakage current in solutions containing TBAH. Left: Normal sample without additional insulation. Right: New sample type with thin leads and polyimide insulation. The dashed line shows the current expected from a $10^{-5}\,G_0$ linear conductance.

3.1.1. Determining Operational Parameters for IV Measurements

IV measurements were first performed in the following way. The push rod was slowly moved up and down, opening and closing the junction, at a speed of typically 5 µm/s while the conductance was measured at a low bias voltage (typically 0.1 V). When the conductance trace reached a plateau or an interesting value, the motor was stopped and the IV measurement started. Thereby the voltage was slowly ramped (typically 2 V/s) up and down in small steps of 10 mV. The voltage ramp started at the value which was used for conductance measurements and also ended at this value after typically 5 cycles. It was found that high bias voltages increase the probability for the junction to suddenly close due to electrostatic forces between the electrodes or gold atoms moved by the large fields. A closed junction will quickly be damaged by large voltages and associated large currents leading to electromigration and/or melting. The series resistor between voltage source and sample was increased from 1 kΩ to 100 kΩ in order to prevent this damage. Figure 3.3 shows two IV measurements obtained in a 1 mM solution of 1-octanethiol in mesitylene with a ramp speed of 2 V/s. The IV curves are quite stable for a bias range of ±2.0 V (left) but show strong fluctuations at higher voltages (right). Octanemonothiol cannot bridge the junction but it forms stable monolayers on the electrodes which might mechanically stabilise them. In a comparison to IV measurements in pure solvents (not shown), octanemonothiol did indeed seem to stabilise the junctions but as the stability changes between junctions and over time this

cannot definitely be attributed to the molecule. The curves recorded with ±2.5 V show a tendency of closing (sharp increases of the currents in the black and green curves).

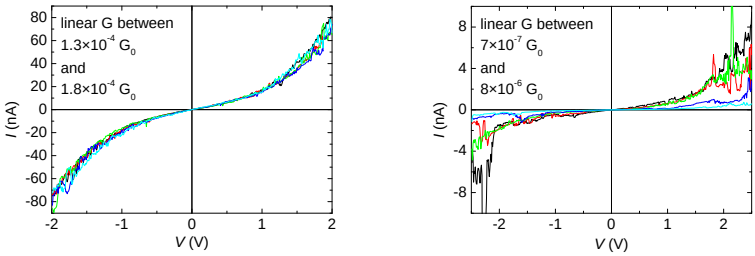

Figure 3.3.: IV measurements in 1 mM of octanemonothiol in mesitylene with a ramp speed of 2 V/s. Bias range of ±2.0 V (left) and ±2.5 V (right), both measurements were performed with the same junction. Strong current fluctuations are observed at voltages above 2.0 V.

An IV measurement of 0.25 mM S-OPE-S in THF/mesitylene 1:4 is shown in figure 3.4 (left). For these measurements, the voltage ramp was started along a conductance plateau after stopping the push rod. The low-bias conductance was obtained from linear fits of the IV curves over a range of ±0.1 V. A histogram of those values is shown in figure 3.4 (right) and compared to normal opening curve histograms (see section 1.3) from the same sample. The position of the histogram peaks coincide nicely.

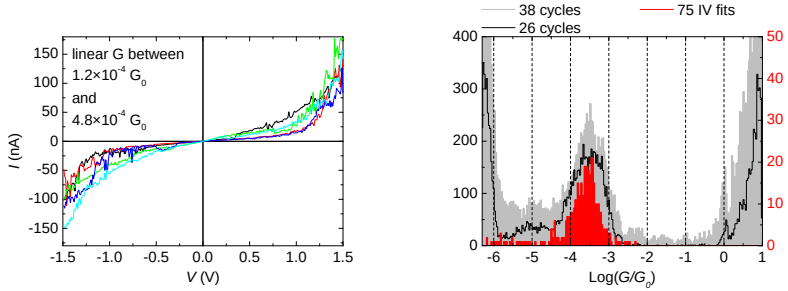

Figure 3.4.: Left: IV measurement of S-OPE-S 0.25 mM in THF/mesitylene 1:4. Right: Conductance histogram obtained from linear fits to 75 IV curves (red) compared to histograms from normal opening cycles measured before (grey) and after the IV curves (black).

The method of manually stopping along conductance plateaus and then recording IV curves works in principle but it has disadvantages: The beginning of the plateau is not available for the IV measurement as a plateau has to be identified before the voltage ramp is started. If the measurement is to be started by hand there will be an additional delay during which the molecular junction can break or the distance between the electrodes could change considerably. The linear conductance of the junction is known only once per voltage ramp, when the voltage intersects zero. Any conductance variations happening at a frequency of 1 Hz or faster caused for example by molecules binding and unbinding or 1/f noise are therefore difficult to observe. For these reasons it was decided to develop a method for measuring IV characteristics by continuously ramping the bias voltage at a much faster speed. The technical details are discussed in the subsequent section.

3.1.2. Implementation of a Fast IV Acquisition Setup

Due to the unstable nature of molecular junctions in liquid environments, it is desirable to measure both its the linear conductance at low bias voltage and the IV characteristics at high rates. This would allow to assign IV data to conductance plateaus and even to study the time development of IV curves on a plateau. It has been considered to switch to the shunt resistor method to measure IV curves. The voltages over the current measuring resistor and the sample could then easily be plotted against each other. A disadvantage of this method is the limited bandwidth of the voltage measurement in such a setup. Its cut-off frequency depends mainly on the sample resistance and the capacitance of the cable and amplifier and is given by $\omega_{\text{-3dB,Ibias}} = (R_{\text{sample}} C_{\text{cable,amp}})^{-1}$. Even with very low input capacitance amplifiers and very short cables (or guarding), the achievable bandwidth is well below 1 kHz for a typical sample resistance of 100 MΩ which is not enough for fast IV measurements. Applying the bias voltage through a series resistor and measuring the current by an IV converter does not suffer from this fundamental bandwidth limitation. Here, the cut-off frequency is mainly defined by the bandwidth of the IV converter and is independent of the sample resistance.

The measurement method was implemented as follows. The bias voltage is smoothly ramped in a triangular form at a frequency of 50 Hz with an amplitude of usually 1.5 V. The current is amplified by an IV converter (SP895/SP895a developed in-house, see section B.1) with a gain of 10^7 V/A and a bandwidth of about 10 kHz and sampled at 20 kHz. A National Instruments DAQ board is used for both input and output. While IV data is being recorded continuously, the push-rod motor is controlled by a LabVIEW program to move upwards (opening) at 5 µm/s and downwards (closing) at 50 µm/s. The lower opening speed leads to longer plateaus which allows recording more IV curves whereas

the higher closing speed saves time and increases the probability for the junction to fully re-close (less drift of the electrode tips). The IV data is recorded into a RAM buffer which contains 10 seconds of current data and is flushed to the hard drive on request. In this way, uninteresting data (e.g. with the junction fully closed or fully broken) can be discarded to save space and analysis time. A series resistance in front of the sample limits the current to prevent damage to the junction when closed. Figure 3.5 shows a schematic diagram of the setup.

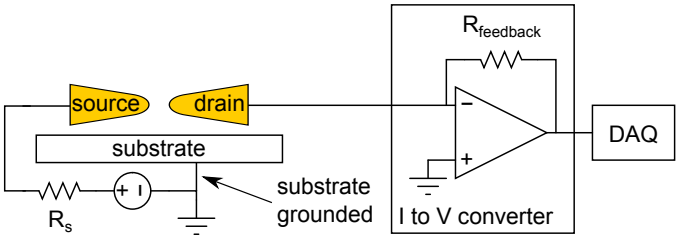

Figure 3.5.: Electric circuit used for fast IV measurements. The fixed bias voltage is replaced by a signal generator, the gain of the IV converter is fixed at 10^7 V/A, the series resistance $R_s = 100\,\mathrm{k}\Omega$ is moved closer to the sample and the sample substrate is connected to ground.

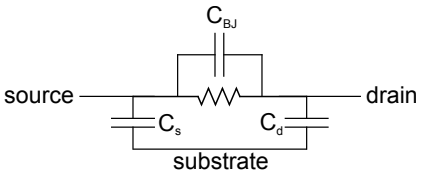

Figure 3.6.: Schematic of the capacitances present in break junction sample on conductive substrates.

When ramping the voltage this quickly, the capacitive current through the sample can dominate the IV data as it increases proportionally to the ramping speed ($I_C = C_{sample}\dot{U}$). A schematic of the capacitances present in the break junction samples is given in figure 3.6. The capacitance of the actual junction between the electrode tips (C_{BJ}) is negligible. The capacitances between the source and drain traces and the steel substrate (C_{s} and C_{d}) however are substantial. If the substrate is floating, the two capacitances add up to $C_{\mathrm{sample}} = (C_{\mathrm{s}}^{-1} + C_{\mathrm{d}}^{-1})^{-1}$. The effective capacitance can be greatly reduced by grounding the sample substrate as this prevents any potential difference between the drain part of the gold leads which is connected to the virtual

ground of the IV converter and the metal substrate. Figure 3.7 shows this effect of grounding in both AC frequency response measurements (left) and IV measurements (right) with a fully opened junction. The capacitances calculated from the current frequency response are $C_{\text{floating}} = \frac{I}{U\omega} = 1.1 \cdot 10^{-11}\,\text{F}$ and $C_{\text{grounded}} = 1.5 \cdot 10^{-13}\,\text{F}$. A reduction by a factor of 70. This reduction is also observed in the IV measurement where the current is reduced by a similar factor. In addition to this electronic countermeasure, the capacitive currents of up and down voltage ramps will cancel each other out when averaging several IV curves. It should be mentioned that while most IV measurement methods reported in the literature use the technique of stopping the movement on plateaus before ramping the bias voltage [29, 30], a method very similar to the one developed in this work was presented by Hong et al. [31].

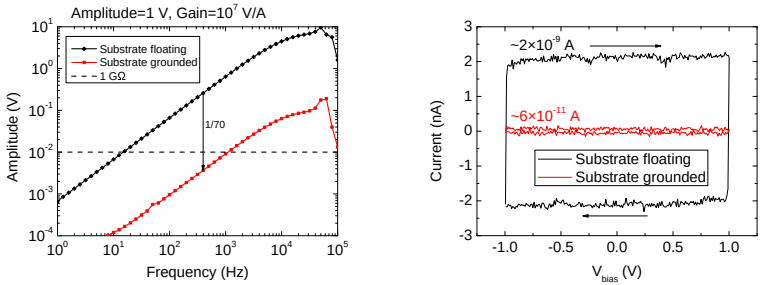

Figure 3.7.: Left: Frequency response of a fully opened junction with the substrate floating and grounded. The dashed line indicates an Ohmic sample resistance of 1 GΩ. Right: Corresponding IV data showing the source drain current.

3.2. IV Characteristics of Symmetric and Asymmetric Molecules

Three derivatives of oligo(phenylene ethynylene) (OPE) have been chosen as an interesting test case for IV measurements. The molecular structures are shown in figure 3.8. All three molecules consist of an identical aromatic core structure but contain different linker groups. Both the sulphur and pyridine groups are known to reliably bind to gold but with different bonding properties. It is particularly interesting about this set of molecules that it contains both the symmetrical variants S-OPE-S and N-OPE-N and the asymmetrical variant N-OPE-S. 0.25 mM solutions of the molecules in THF/mesitylene 1:4 were used for the measurements. In the cases with sulphur linkers the solution was bubbled

with argon and TBAH was added to remove the acetyl protection groups as discussed in section 1.3.

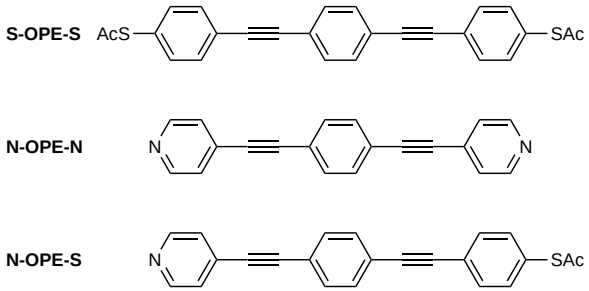

Figure 3.8.: Chemical structure of the three OPE variants measured. S-OPE-S with two acetyl-protected sulphur linker groups, N-OPE-N with two pyridine linkers and N-OPE-S with one of each linkers.

The measurements were performed as described in section 3.1.2. Figure 3.9 gives an overview of the data obtained for all molecules. In the top row, 2D histograms show the conductance – distance relationship of opening traces. The conductance values in these plots have been obtained from linear fits of individual IV traces in the range of $\pm 0.2\,\mathrm{V}$.[1] A typical single $G(z)$ curve is overlaid for each molecule (black, with the plateau highlighted in red). The middle row shows all the IV curves along the plateau marked in the typical opening trace shown for each molecule in red. The average IV curve is shown in black. Each of the red IV curves corresponds to one data point in the conductance traces. In the bottom row the same conductance data from IV measurements is presented as 1D histograms (red) and compared to fixed bias (0.1 V) data (black). The peak positions in the conductance histograms from IV and fixed bias measurements agree approximately but there appears to be a trend for the IV data to show plateaus at a slightly higher conductance. This is most visible in the N-OPE-N histograms. The reason for this difference in conductance is not yet fully understood. It seems to be of microscopic origin as it varies between junctions. Presumably due to the larger bias voltage in IV measurements the formation of more stable junctions is favoured (apparent in the more prominent peaks in the 1D histograms). Those more stable junctions are likely to also have a higher conductance. The typical IV curves of S-OPE-S and N-OPE-N are symmetric whereas a clear asymmetry is seen in the N-OPE-S

[1] Due to the fast nature of the voltage ramp, the frequency response of the amplifier has to be taken into account in order go obtain correct conductance values for closed junctions ($G \geq G_0$). See section B.2 for details.

case. This is clear evidence that the shape of the IV curve is directly influenced by the molecular structure. In the following section, a model is developed to describe the transfer through all measured molecules. The model is then applied to systematically analyse a large number of IV curves from the three molecules.

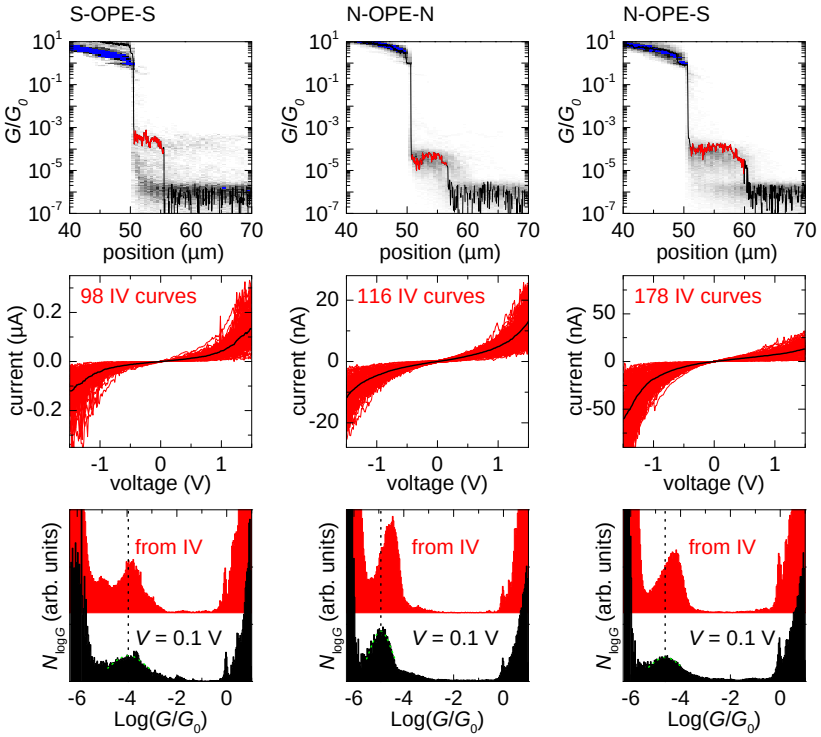

Figure 3.9.: Data for S-OPE-S, N-OPE-N and N-OPE-S (left to right). Top row: 2D conductance histograms constructed via opening traces obtained from IV data (background). One typical conductance trace per molecule is shown as black and red line. The conductance plateau along which the IV curves were obtained is highlighted in red. Second row: Individual IV traces obtained on the indicated plateau (red). The average IV is shown in black. Bottom row: 1D conductance histograms from IV data (red) compared to histograms from fixed bias data (black).

3.3. Single Energy Level Model

Several models have been employed to describe single molecular junctions. Simmons' tunnelling formula [32] was used to model the junction as a rectangular barrier and the transition voltage spectroscopy was applied to IV measurements [33, 34]. It was shown, however, that the Simmons model is inconsistent with molecular IV measurements and that a single level model should be used to interpret transition voltages [35]. It is possible to fit a single level model directly to IV data and to omit the detour to transition voltage spectroscopy. That approach is used in this work. An analytical model with three independent physically meaningful parameters is employed that describes the IV curves accurately.

The simple single level model used in this work assumes a situation as sketched in figure 3.10 [36–39]. The transport is dominated by a single molecular energy level E_0 (either HOMO or LUMO) and the voltage drops exclusively over the contacts which are described by the coupling constants Γ_1 and Γ_2 (independent of V). The energy level is broadened by the coupling to the electrodes and its density of states is then described by a Lorentz or Breit-Wigner distribution (equation 3.1). In our model, the average Fermi level of the two electrodes is set to 0 and all energies in the problem are relative to this Fermi level. For the symmetric case $\Gamma_1 = \Gamma_2$, the "Fermi level" of the molecule E_F will also stay fixed at 0 for $V \neq 0$ so $E_0(V) = E_0$.

$$D_e(E) = \frac{(\Gamma_1 + \Gamma_2)/\pi}{(E - E_0(V))^2 + (\Gamma_1 + \Gamma_2)^2} \tag{3.1}$$

The transmission function of the system is obtained from the density of states and the coupling constants:

$$T(E, V) = 4\pi D_e(E) \frac{\Gamma_1 \Gamma_2}{\Gamma_1 + \Gamma_2} \tag{3.2}$$

$$T(E, V) = \frac{4\Gamma_1 \Gamma_2}{(E - E_0(V))^2 + (\Gamma_1 + \Gamma_2)^2} \tag{3.3}$$

Shift from coupling and bias voltage

In the asymmetric case ($\Gamma_1 \neq \Gamma_2$), $E_F \neq 0$ is expected for $V \neq 0$. A full treatment of $E_F(V)$ requires knowledge of the contact capacitances, polarisability of the molecule and should take into account the bias dependence of the coupling constants. However, a reasonable linear approximation can be derived as follows.

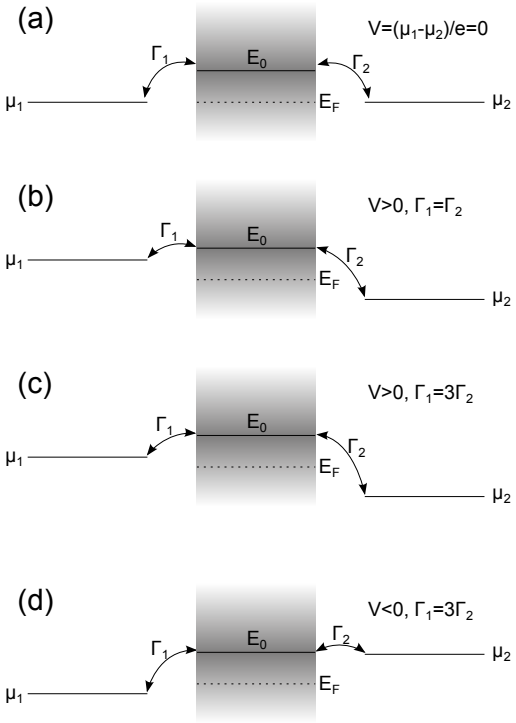

Figure 3.10.: Sketch of the energy levels in the single level model for the LUMO case. (a) $V = 0$. (b) $V > 0$ for identical coupling constants. (c) $V > 0$ for $\Gamma_1 > \Gamma_2$, far from resonance, low current. (d) $V < 0$ for $\Gamma_1 > \Gamma_2$, close to resonance, high current.

The voltage drops are forced to be $\propto \Gamma^{-1}$

$$\frac{\frac{eV}{2} - E_F(V)}{\frac{eV}{2} + E_F(V)} \stackrel{!}{=} \frac{{\Gamma_1}^{-1}}{{\Gamma_2}^{-1}} \tag{3.4}$$

This directly leads to a reasonable voltage dependence of the molecular Fermi level

$$E_F(V) = \frac{eV}{2} \cdot \frac{\Gamma_1 - \Gamma_2}{\Gamma_1 + \Gamma_2} \tag{3.5}$$

and therefore of the molecular energy level.

$$E_0(V) = E_0 + E_F(V) = E_0 + \frac{eV}{2} \cdot \frac{\Gamma_1 - \Gamma_2}{\Gamma_1 + \Gamma_2} \tag{3.6}$$

Equation 3.5 can also be interpreted as E_F shifting away from the average Fermi levels of the electrodes towards the Fermi levels of the electrodes. The amount of shift is weighted by the coupling constants so the level finally shifts towards the better coupled electrode. The relationship fulfils the following reasonable boundary conditions and is linear in between:

- $E_F = 0$ for $\Gamma_1 = \Gamma_2$
- $E_F = eV/2 = \mu_1$ for $\Gamma_1 \gg \Gamma_2$ and $E_F = \mu_2$ for $\Gamma_2 \gg \Gamma_1$

With the transmission function as defined by equation 3.3, the current is obtained from the Landauer formula [36] and reads

$$I(V) = \frac{2e}{h} \int_{-\infty}^{\infty} T(E,V)[f(E - eV/2) - f(E + eV/2)]dE \tag{3.7}$$

At low temperatures, the two Fermi functions can be approximated by Heaviside step functions. Now the current can be expressed as a finite integral

$$I(V) = \frac{2e}{h} \int_{\frac{-eV}{2}}^{\frac{eV}{2}} T(E,V)dE \tag{3.8}$$

which evaluates analytically:

$$\begin{aligned} I(V) = \frac{8e}{h} \cdot \frac{\Gamma_1\Gamma_2}{\Gamma_1 + \Gamma_2} \Bigg[&\arctan\left(\frac{2E_0 + eV\frac{\Gamma_1 - \Gamma_2}{\Gamma_1 + \Gamma_2} + eV}{2(\Gamma_1 + \Gamma_2)}\right) \\ &- \arctan\left(\frac{2E_0 + eV\frac{\Gamma_1 - \Gamma_2}{\Gamma_1 + \Gamma_2} - eV}{2(\Gamma_1 + \Gamma_2)}\right)\Bigg] \end{aligned} \tag{3.9}$$

This low temperature approximation is valid even for coupling constants Γ_1 and Γ_2 considerably lower than the thermal broadening of the Fermi functions at room temperature $k_BT = 25\,\text{meV}$. The reason is that the Breit-Wigner distribution of the density of states decays slowly ($\propto E^{-2}$) whereas the Fermi functions decay quickly with $\exp(-E)$ and the integration range does not contain the density of states maximum (no resonant transport). Therefore the thermal broadening of the Fermi levels in the electrodes is negligible compared to the broadening of the molecular level by coupling. This fact is elaborated in section C.1. In the case of resonant transport, thermal broadening should be taken into account [37].

3.4. Systematic Investigation of Symmetric and Asymmetric Molecules

Equation 3.9 was fitted to IV curves obtained on plateaus. Figure 3.11 shows fits to two of the example IV curves shown in figure 3.9 (N-OPE-N and N-OPE-S). The data is well-described by the model and the three fitting parameters E_0, Γ_1 and Γ_2 can be extracted.

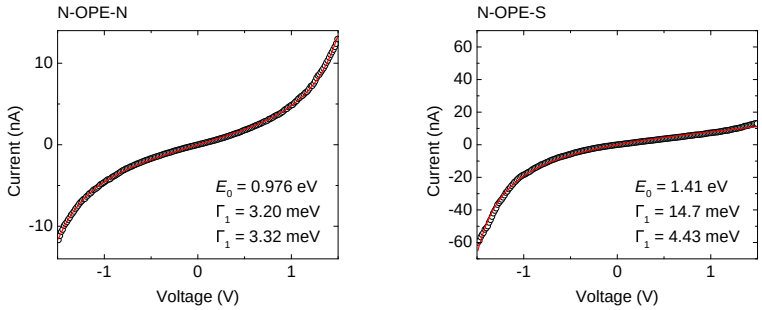

Figure 3.11.: IV data averaged along a plateau as shown in figure 3.9 for N-OPE-N and N-OPE-S (open circles) and a fit with the single level model (red line). The extracted fitting parameters are indicated.

For a statistical analysis of the IV data, conductance plateaus in opening curves were identified by hand. The IV curves along one plateau were then averaged and fitted by the model.A total of 51, 205 and 183 averaged IV curves were analysed for S-OPE-S, N-OPE-N and N-OPE-S, respectively to obtain a distribution for each of the fitting parameters. Figure 3.12 shows the distributions of the fitting parameters. The energy level E_0 (a) shows quite a narrow distribution for both S-OPE-S ($\approx 0.9\,\text{eV}$) and N-OPE-N ($\approx 1.0\,\text{eV}$)

whereas it is spread between 0.8 eV and 1.7 eV for N-OPE-S. The coupling constants show a larger spread which is why they are shown in a logarithmic histogram (b). For each molecule, the histograms show the lower of the two Γ at the bottom and the higher one at the top. The distributions of Γ_{high} and Γ_{low} are very similar for the symmetric S-OPE-S and N-OPE-N whereas they significantly differ for N-OPE-S.

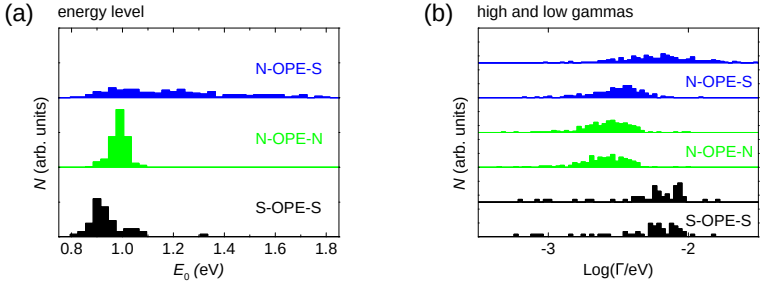

Figure 3.12.: Distribution of the position of the energy level E_0 (a) and of the high and low coupling constants Γ_{high} and Γ_{low} (b) from all IV fits.

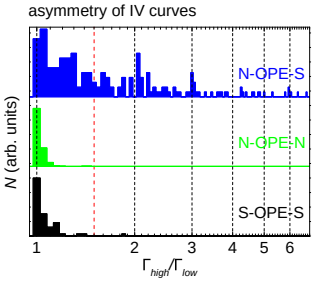

Figure 3.13.: Distribution of $\Gamma_{\mathrm{high}}/\Gamma_{\mathrm{low}}$ indicating the asymmetry of the IV curves. The histogram counts are normalised to the number of counts at 1. The threshold used to select asymmetric curves is indicated by the red dashed line.

Figure 3.13 show the distribution of $\Gamma_{\mathrm{high}}/\Gamma_{\mathrm{low}}$ for each molecule. Most values are close to 1 for S-OPE-S and N-OPE-N with very few values being significantly larger. For N-OPE-S the most probable value is also close to 1 but the spread is much larger which reflects the frequently observed asymmetry in IV curves for this molecule. As single molecular junctions of N-OPE-S are expected to mostly show asymmetric IV characteristics, those with $\Gamma_{\mathrm{high}}/\Gamma_{\mathrm{low}} > 1.5$ were

selected for further analysis. This threshold was chosen such that it is very rarely reached by the data from the symmetric molecules but does not exclude a large amount of asymmetric data from the analysis. 60 % from the total of 183 IV curves for N-OPE-S exceed this asymmetry threshold. Figure 3.14 shows this selected data compared to the data taken from figure 3.12 for the symmetric molecules. The most striking observation in the E_0 distribution (a) is that the most probable value is now clearly higher than for the symmetric molecules with zero counts below 1.0 eV. In the distribution of the coupling constants, Γ_{high} and Γ_{low} are now more clearly separated. The observed range of Γ_{high} matches the distribution for S-OPE-S quite well whereas Γ_{low} is in close agreement to the N-OPE-N data.

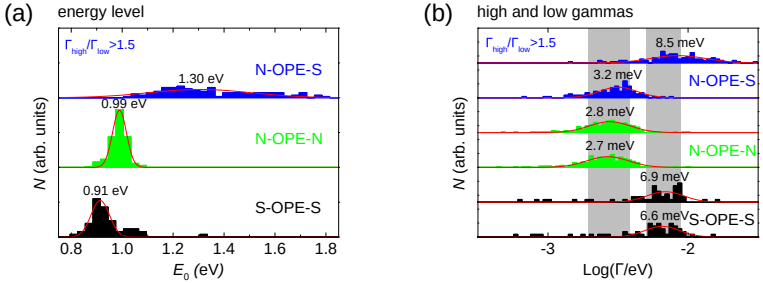

Figure 3.14.: Distribution of the position of the energy level E_0 (a) and of the high and low coupling constants Γ_{high} and Γ_{low} (b) from all IV fits of S-OPE-S and N-OPE-N. For N-OPE-S, asymmetric curves have been selected ($\Gamma_{\mathrm{high}}/\Gamma_{\mathrm{low}} > 1.5$). Gaussian fits to the distributions are shown in red and the peak values are given. In (b), the average peak values for S-OPE-S and N-OPE-N and are indicated as grey areas in order to compare them to the N-OPE-S distributions.

The fact that both coupling constants for N-OPE-S match the respective values for the symmetric molecules is evidence for the power of the single level model. Despite its simplicity it describes the data well enough to separate effects of different coupling from different energy level positions. It might seem surprising at first that E_0 is significantly larger for N-OPE-S than for the symmetric molecules but this observation can be explained in the way sketched in figure 3.15. E_0 is the distance of the dominant (closer) energy level to the Fermi energy and will therefore be negative and positive for the LUMO (a) and HOMO (b) case, respectively. Due to the symmetry of the Breit-Wigner distribution only the absolute value of E_0 can be obtained by fitting the single level model to IV data and the sign will be neglected from here on. From UV-vis absorption spectra of S-OPE-S in solution, the HOMO-LUMO gap ΔE is estimated to be ≈ 3.5 eV [6]. We assume that ΔE is similar for N-OPE-N

and N-OPE-S and that the difference in E_0 is mainly due to different alignment of the molecular energy levels relative to the Fermi energy of the electrodes. The alignment in the case of N-OPE-S is expected to lie in between the cases for S-OPE-S and N-OPE-N. It can be deduced from the observed values for E_0 that the HOMO level is dominant for one of the symmetric molecules whereas the LUMO level is dominant for the other one. $E_{0,\mathrm{NS}}$ is then expected to be larger than both $E_{0,\mathrm{SS}} \approx 0.9\,\mathrm{eV}$ and $E_{0,\mathrm{NN}} \approx 1.0\,\mathrm{eV}$. The maximum possible value would be $E_{0,\mathrm{NS,max}} = \Delta E/2 \approx 3.5\,\mathrm{eV}/2 = 1.75\,\mathrm{eV}$ if the alignment is as in figure 3.15c. The distribution shown in figure 3.14 fulfils these requirements with the most probable value at 1.2 eV and a largest value of 1.8 eV.

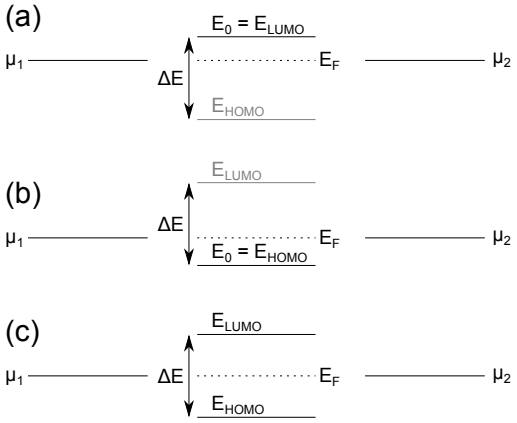

Figure 3.15.: Proposed alignment of the molecular energy levels. (a) Case of LUMO transport, e.g. for N-OPE-N. (b) Case of HOMO transport, e.g. for S-OPE-S. (c) Alignment between the N-OPE-N and S-OPE-S case expected for N-OPE-S with either HOMO or LUMO transport but definitely a larger E_0.

We therefore conclude that a different molecular orbital is dominant for the charge transport through S-OPE-S and N-OPE-N. This is in agreement to theoretical and experimental (thermopower) studies where thiol-linked molecules have been shown to conduct through the HOMO whereas the LUMO was shown to dominate in the pyridine case [40, 41].

3.5. Development of IV Characteristics on Plateau

The fast and continuous measurement of IV curves allows to investigate the development of their properties on single conductance plateaus. Figure 3.16 shows the development of the conductance and the three fitting parameters of

the single level model along plateaus for S-OPE-S (a) and N-OPE-N (b). The average of 4 IV curves (2 up and 2 down ramps) was fitted to the model. The averaging was employed to reduce noise and thereby increase the reliability of the fits. In the plots it is seen that changes in the conductance (connected blue squares) correlate strongly with changes in the coupling constants Γ_1 (red triangles) and Γ_2 (green triangles) whereas the energy level E_0 (black squares) stays constant during conductance changes. In those examples the IV curves are predominantly symmetric ($\Gamma_1 \approx \Gamma_2$). Short intervals of asymmetry are observed after the middle of the plateau for S-OPE-S and at the beginning of the plateau for N-OPE-N (indicated by arrows). Note that the single level model is not suitable for describing the IV data recorded before the molecular plateau (especially when $G \geq 1G_0$) and after the plateau (tunneling and leakage current) as it does not describe these situations. The fitting parameters obtained in these regimes (shaded in grey) are therefore not physically meaningful.

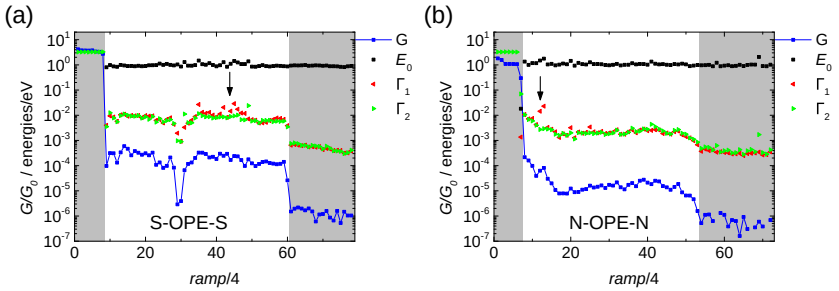

Figure 3.16.: Fitting parameters along a plateau for S-OPE-S (a) and N-OPE-N (b). 4 IV curves (2 up and 2 down ramps) were averaged for each fit. Both data contain predominantly symmetric curves ($\Gamma_1 \approx \Gamma_2$) except for short intervals indicated by arrows.

Two measurements for N-OPE-S are presented in figure 3.17. In (a) a typical example is shown with a strong asymmetry throughout the plateau. Some of the obtained coupling constants are unreasonably large or small (examples indicated by arrows). The reason for these outliers is that the single level model is not very robust for strongly asymmetric IV curves and is susceptible to noise or sudden jumps. See section C.3 for an illustration of this problem. In some rare cases, abrupt changes in the asymmetry are observed as seen in (b). Here the IV characteristics switch from more current at positive bias voltage (A_1) to approximately symmetric (S) and then to more current at negative bias voltage (A_2) during a single conductance plateau.

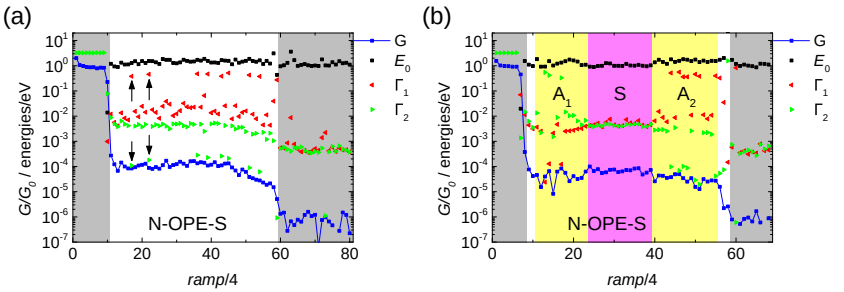

Figure 3.17.: Fitting parameters along a plateau for N-OPE-S. 4 IV curves (2 up and 2 down ramps) were averaged for each fit. Continuous asymmetry is the most common case (a) while switches in the asymmetry are more rarely observed (b).

Figure 3.18 shows the same data with IV curves averaged over intervals chosen by hand. The rectification ratio (shown in the inset) reaches values of about 5 for the blue IV curve. Fits to the single level model are shown as solid lines. The parameters obtained from the fits are listed in the caption. The sum of the asymmetric red and blue IV curves is shown as pink squares. It matches the symmetric green IV curve very closely.

This switching between symmetry and asymmetry can be explained as follows. In the red interval a single N-OPE-S molecule bridges the gap between the electrodes which leads to an asymmetric IV curve. During the green interval an additional molecule bridges the gap in the opposite direction. The two antiparallel asymmetric molecules add up to an approximately symmetric IV characteristic. Note that the single level model does in principle not apply to this situation as two molecules are involved but the obtained coupling constants can still be used as a measure of asymmetry. In the blue interval the first molecule has lost at least one of its bonds to the electrodes and does not significantly contribute to the transport any more. This results in an IV curve of a polarity opposite to the red one. This explanation is strongly supported by the fact that the sum of the asymmetric red and blue IV curves (shown in pink) matches the symmetric green IV curve.

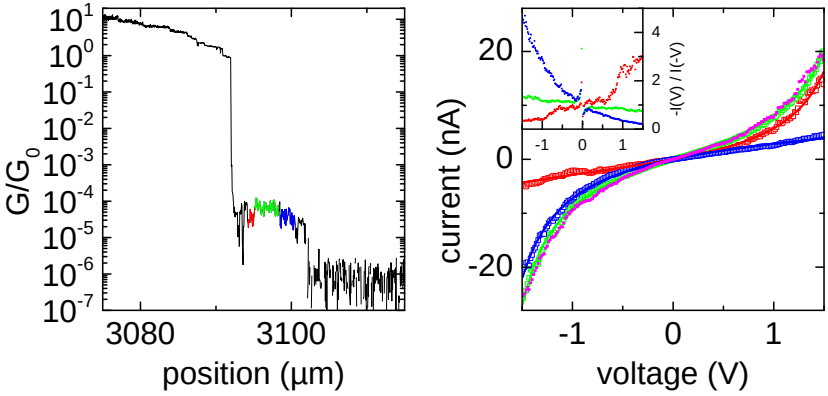

Figure 3.18.: Same data as on the right of figure 3.17. Three intervals with approximately constant IV curves were chosen by hand and are indicated by colors. The averages of those IV curves are shown on the right (boxes of matching colors). Fits to the single level model are shown as solid lines. The fitting parameters are (red) $E_0 = 1.37\,\text{eV}$, $\Gamma_1 = 2.99\,\text{meV}$, $\Gamma_2 = 6.98\,\text{meV}$, (green) $E_0 = 0.972\,\text{eV}$, $\Gamma_1 = 4.56\,\text{meV}$, $\Gamma_2 = 4.18\,\text{meV}$, (blue) $E_0 = 1.62\,\text{eV}$, $\Gamma_1 = 12.9\,\text{meV}$, $\Gamma_2 = 2.55\,\text{meV}$. The sum of the red and blue IV curves is shown as pink squares. Inset: The rectification ratio $-I(V)/I(-V)$ as a function of bias voltage.

3.6. Conclusions

A method to acquire IV curves during opening and closing cycles of a MCBJ in liquid has been developed. IV characteristics of symmetric and asymmetric variants of OPE have been measured. The symmetric molecules lead to predominantly symmetric IV curves whereas rectification ratios of up to ≈ 5 are observed for N-OPE-S at $\pm 1.5\,\mathrm{V}$. The IV curves were accurately described by a single level model with three fitting parameters: The position of the dominant molecular energy level and the two coupling constants could be obtained for the measured molecules. The comparison of those parameters between the molecules validates the single level model. In particular, the difference in the molecular energy levels was used to demonstrate that transport through the molecules is dominated by different molecular orbitals for the two symmetric molecules (LUMO vs. HOMO). The measuring technique is fast enough to observe changes in the IV characteristics along a single conductance plateau. Some examples of such changes provide strong evidence for the transport to be dominated by single molecules.

Chapter 4

The Effect of Polar Anchor Groups

In this chapter, biphenyl molecules with isocyanide, cyanide and sulphide anchor groups are compared to see the effect of different linker groups on junction formation and conductance. The diisocyanides of naphthalene and benzene are also measured to investigate length dependence. Figure 4.1 shows the structure of the molecules with the abbreviations used from here on.

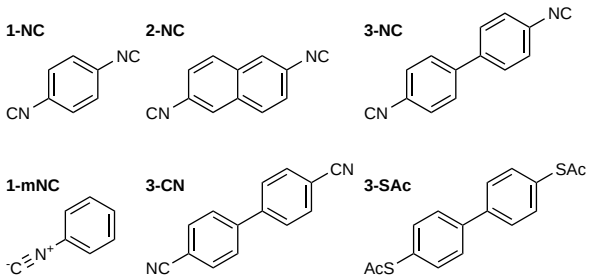

Figure 4.1.: Chemical structures of the molecules investigated in this chapter. 1-NC: phenyl diisocyanide, 2-NC: napthalene diisocyanide, 3-NC: biphenyl diisocyanide, 1-mNC: phenyl monoisocyanide, 3-CN: biphenyl dicyanide, 3-SAc: biphenyl dithiol.

The isocyanide group is an interesting candidate as linker for molecular junctions. It is known to bond at steep angle of 24° from surface normal to gold surfaces [42]. This is different from thiols which also allow a molecule to lie flat on the metal surface. Another property inherent to isocyanide groups is their dipole moment which results from the partial triple bond character of the N–C bond [43]. This dipole could lead to a reduction of the metal electrode work function [44] and could be imagined to cause an attractive force

between molecules. Strong gradients in the electric field could also act on the isocyanide dipoles even in symmetric molecules with no global dipole moment. While isocyanides are known as a linker group in molecular electronics [45–48], they have not been investigated as thoroughly as thiols, pyridines or amines [5, 7, 27, 47, 49, 50].

4.1. Comparison of Thiol, Isocyanide and Cyanide Linker Groups

Opening and closing conductance traces of symmetric biphenyl molecules were measured with a fixed bias voltage of 0.1 V. The push rod speed was 31.2 µm/s and the concentration was 0.25 mM in THF/mesitylene 1:4. Argon was bubbled through the solution to purge oxygen. TBAH in THF was added to remove the protection group from the sulphur linkers. Biphenyl molecules with sulphur linker groups were successfully measured before in STM setups both in solution [51] and with self-assembled monolayers in vacuum [47]. Their lengths are in the range of other molecules successfully measured with the MCBJ setup used in this work. Therefore, 3-SAc was expected to show clear conductance plateaus. For 3-NC, only measurements of monolayers in vacuum were found in literature [47, 48]. In order to better assess the effect of the linker group on transport, we present in this paragraph a systematic comparison between 3-SAc, 3-NC and 3-CN.

Opening and closing curves for 3-SAc are shown in figure 4.2. In (a), typical opening curves both with and without plateaus and a 2D histogram of 500 consecutive opening curves are presented. Plateaus are observed around $1.4 \cdot 10^{-3}\, G_0$ in about 30 % of the curves. This conductance value is obtained from the histogram of the curves showing plateaus (figure 4.3, G_1 in table 4.1) and indicated as horizontal dashed line. Curves with and without plateaus correspond to the two bundles observed in the 2D histogram (right). The two bundles are indicated by dashed ellipses. The closing traces presented in b) show the expected exponential increase of the conductance with decreasing distance except for a few outlier curves where the junction was closing much slower at a conductance of about $5 \cdot 10^{-2}\, G_0$ (one example shown on the left). In the 2D histogram this translates to a high density along an approximately straight line (emphasised in red) except for the outlier curves. Outliers with slow changes in conductance can show in both opening and closing curves for different molecules. They typically represent between 0 and 10 % of all curves (more when the sample is not working correctly) and are attributed to mechanical effects such as, for example, gold particles between the electrode tips or thin flexible tips that are deformed by monolayers that resist junction closing up to a large force. In this work such outlier curves are excluded from the 1D conductance histograms

as they can have a strong effect on the statistics. They are included in the 2D histograms where they can easily be distinguished from the main shape of the distribution.

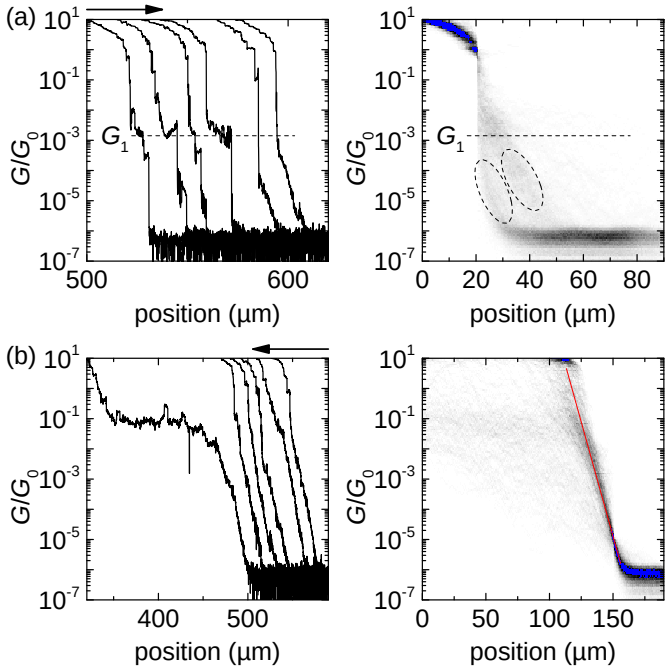

Figure 4.2.: (a) Typical opening curves of 0.25 mM 3-SAc in THF/mesitylene 1:4 both with plateaus (first four from the left) and without (left) and a 2D histogram of 500 consecutive opening curves (right). Plateaus are observed around $G_1 = 1.4 \cdot 10^{-3}\, G_0$ in approximately 30% of the curves. The dashed line indicates the conductance value G_1 as obtained from the histogram peak (figure 4.3). (b) Typical closing curves of 3-SAc with one slowly closing outlier (left) and a 2D histogram of 500 consecutive closing curves aligned at $10^{-5}\, G_0$. The conductance increases approximately exponentially as indicated by the red line. The conductance traces are shifted horizontally for clarity.

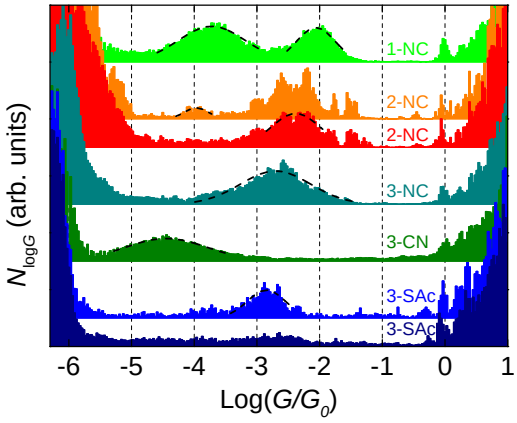

Figure 4.3.: Conductance histograms from opening curves of all the molecules investigated in this chapter normalized to the number of curves. The Gaussian fits used to obtain the conductance values presented in table 4.1 are shown as black dashed lines. 3-SAc: Data from 50 consecutive curves shown in dark blue, data from 13 selected curves with plateau shown in blue. 3-CN: Data from 200 consecutive curves. 3-NC: Data of 100 consecutive curves. 2-NC: Data from 43 consecutive curves shown in red, data from 19 curves selected for the $1.1 \cdot 10^{-4}\, G_0$ plateaus shown in orange. 1-NC: Data from 195 out of 200 consecutive opening curves (also shown in figure 4.7).

In the measurement of 3-NC, shown in figure 4.4, more than 90 % of the opening curves (a) show a conductance plateau around $G_1 = 2.0 \cdot 10^{-3}\, G_0$. This is reflected in the 2D histogram for 100 consecutive curves (right) which shows only one bundle of curves. Apart from the slightly higher conductance and higher plateau yield, the opening curves look similar to the ones from 3-SAc. The closing curves however (bottom) are strikingly different from the disulphide case. They show a reproducible jump from $\approx 1 \cdot 10^{-5}\, G_0$ to $\approx 1 \cdot 10^{-3}\, G_0$ and a slow increase in conductance during further closing. The end of the jumps corresponds to approximately G_1. These conductance jumps are also nicely seen in the 2D histogram (right). The curves were aligned at $5 \cdot 10^{-5}\, G_0$ which is in-between the start and end values of the conductance jumps. Even though all the curves overlap at this conductance value there is no high number of counts at this point which reflects the sharpness and frequent occurrence of the jump. Upon close examination, additional plateaus are marginally visible in the opening curves around $G_2 \approx 2 \cdot 10^{-6}\, G_0$ but mostly buried in the background noise of the setup.

Figure 4.5 shows a measurement of 3-CN. The molecule shows conductance plateaus at $G_1 = 3.6 \cdot 10^{-5}\, G_0$ in about 70 % of the opening curves (a). When closing (b), conductance jumps are observed in some of the curves but not as often as in the isocyanide case which is why they are not seen in the 2D histogram.

In this section opening and closing conductance traces of 3-SAc, 3-NC and 3-CN were systematically compared. It is observed that the conductance plateaus in opening traces are the highest for 3-NC with a value of $G_1 = 2.0 \cdot 10^{-3}\, G_0$. The conductance of 3-SAc junctions is slightly lower at $G_1 = 1.4 \cdot 10^{-3}\, G_0$ and 3-CN shows the lowest conductance of $G_1 = 3.6 \cdot 10^{-5}\, G_0$. The conductance of 3-SAc obtained in this work is higher than what was measured by Mishchenko et al. in an STM setup with the same concentration and solvent mixture [51]. One reason for this difference is that the peak position in the logarithmic conductance histogram is used in the present work [6]. Another reason is the different favoured geometry of the contacts in MCBJ as opposed to STM setups [23, 27]. The very reliable jump to molecular contact in closing curves is observed reliably only for the isocyanide case (3-NC) and is a surprising property of this molecule. The close to perpendicular angle of isocyanide molecules relative to a gold surface are thought to be the reason for the reliable jump to contact. The upright arrangement of the molecules would make a spontaneous bridging while closing the junction much more likely than an arrangement at a flatter angle where more movement of the molecule is necessary. Additionally, 3-NC shows marginally visible additional conductance plateaus around $G_2 \approx 2 \cdot 10^{-6}\, G_0$. Motivated by these surprising observations, two shorter isocyanide molecules were investigated in addition as reported in the following sections.

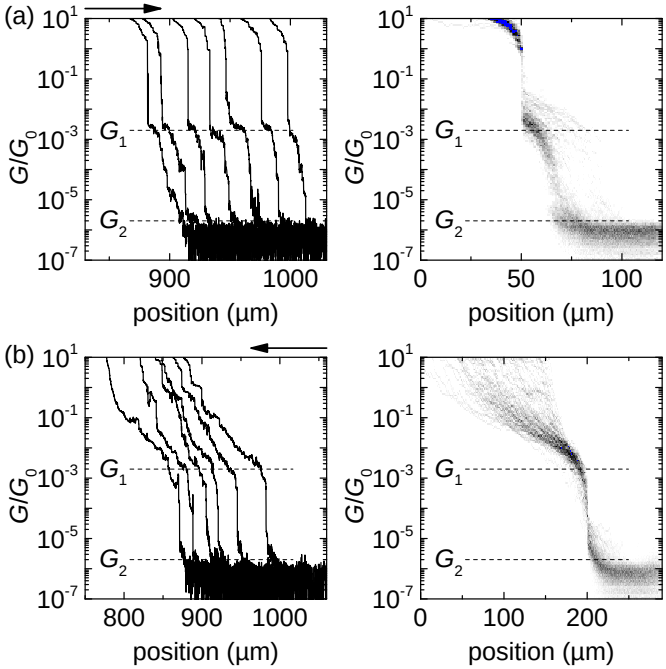

Figure 4.4.: (a) Typical opening curves of 3-NC 0.25 mM in THF/mesitylene 1:4 (left) and a 2D histogram of 100 consecutive opening curves (right). Plateaus are observed around $G_1 = 2.0 \cdot 10^{-3}\, G_0$. Additionally, plateaus are marginally visible around $G_2 \approx 2.0 \cdot 10^{-6}\, G_0$ close to the background noise. (b) Typical closing curves of 3-NC (left) and a 2D histogram of 100 consecutive closing curves aligned at $5 \cdot 10^{-5}\, G_0$. Jumps to molecular contacts are observed.

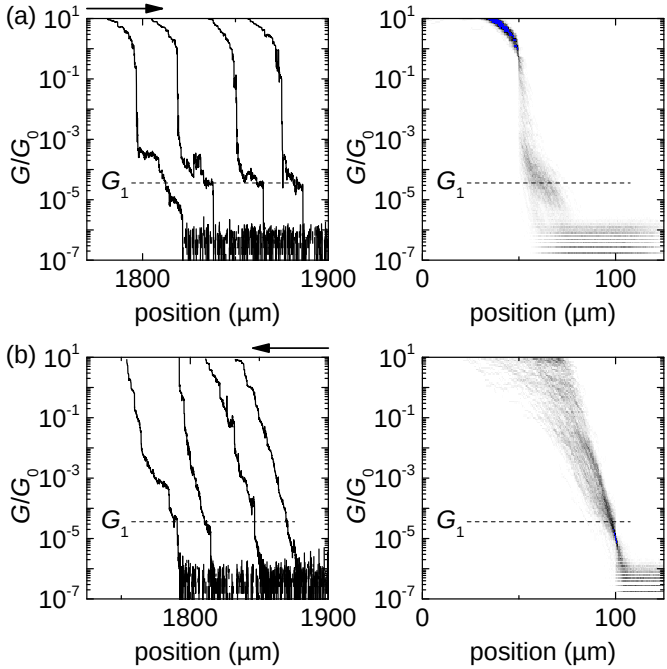

Figure 4.5.: (a) Typical opening curves of 3-CN 0.25 mM in THF/mesitylene 1:4 (left) and a 2D histogram of 200 consecutive opening curves (right). Plateaus are observed around $G_1 = 3.6 \cdot 10^{-5}\, G_0$. (b) Typical closing curves of 3-CN (left) and a 2D histogram of 200 consecutive closing curves aligned at $5 \cdot 10^{-5}\, G_0$. Jumps to molecular contacts are observed in some of the curves but not regularly enough to show in the 2D histogram.

4.2. Evidence for Molecular Chain Formation in Short Isocyanide Molecules

The lower conductance plateau observed for 3-NC is close to the background noise of the setup. 1-NC, which is much shorter than 3-NC, was measured as it was expected to also show lower conductance plateaus at values further from the setup noise. Figure 4.6 shows opening (a) and closing (b) curves on the left and their respective 2D histograms on the right. The opening curves do contain two conductance plateaus around $G_1 = 8.7 \cdot 10^{-3}\, G_0$ and $G_2 = 1.9 \cdot 10^{-4}\, G_0$. The two plateaus show with a probability very close to 1 which gives rise to a clean 2D histogram. The lengths and shapes of the plateaus at the two conductance values are similar. In the rightmost opening curve, a third plateau around $G_3 \approx 3 \cdot 10^{-6}\, G_0$ is seen. Plateaus at this low conductance value close to the background noise are also observed in other curves (the second one shown for example) but are not far enough from noise to be visible in the histograms. Conductance jumps to contact are observed in most closing curves between G_3 and G_2 and between G_2 and G_1. Jumps from background noise to G_3 are also observed in some closing curves as shown in the leftmost curve. The 2D histogram clearly shows the high probability for jumps to the two probable conductance values G_1 and G_2 and a slow closing between and after the jumps. 1D conductance histograms shown in figure 4.7 show two well-defined peaks for both opening (red) and closing (black) curves.

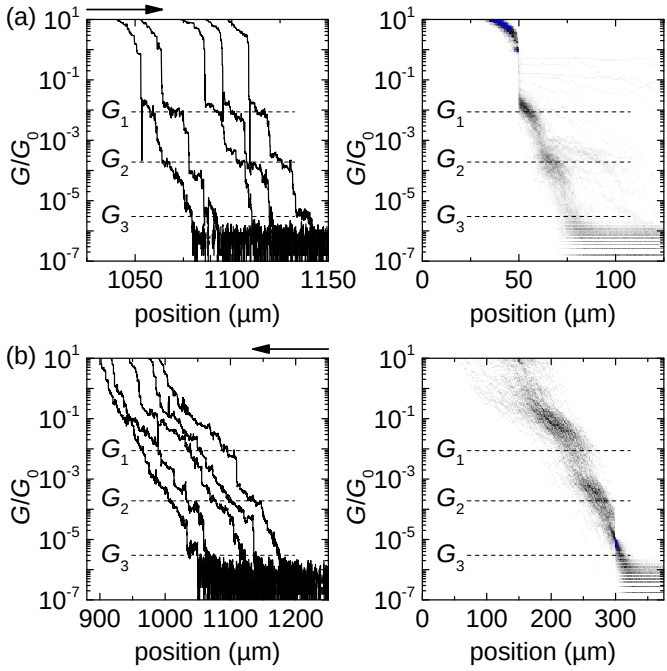

Figure 4.6.: (a) Typical opening curves of 1-NC 0.25 mM in THF/mesitylene 1:4 (left) and a 2D histogram of 200 consecutive opening curves (right). Plateaus are observed around $8.8 \cdot 10^{-3}\,G_0$ and $1.9 \cdot 10^{-4}\,G_0$ in all of of the curves. (b) Typical closing curves of 1-NC (left) and a 2D histogram of 200 consecutive closing curves aligned at $10^{-5}\,G_0$ (right). Jumps to the two conductance values are observed in most curves.

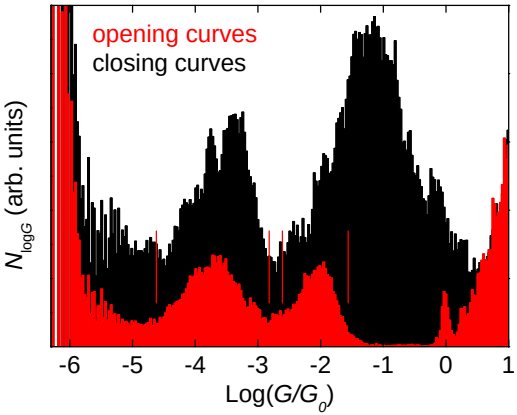

Figure 4.7.: 1D conductance histograms of 1-NC from the data shown in 4.6. 195 out of 200 consecutive opening curves (red) and 200 consecutive closing curves (black).

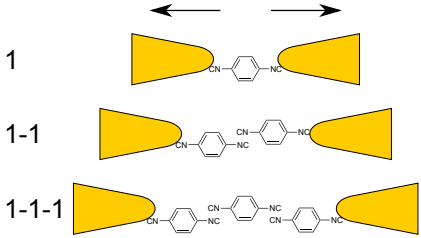

Figure 4.8.: Sketch of the proposed molecular arrangements observed for 1-NC with the designations as used in the text.

The high probability of 1-NC to form molecular junctions could be explained by the close to upright orientation of the molecules on the gold surface. This can help prevent the molecules from bonding to one gold surface with both linker groups. The lower conductance plateaus are interpreted to correspond to chains of two or three molecules in series as sketched in figure 4.8. Attractive dipole–dipole interactions could allow such arrangements as could hydrogen bonds between the isocyanide carbon and a hydrogen of the phenyl ring [52]. This interpretation is supported by the crystal structure of 1-NC shown in figure 4.9 which suggests hydrogen bonds between the molecules. As the molecules are separated by a distance of about 4 Å, transport between them is still be

possible by tunnelling through space but the distance is expected to give rise to an additional barrier. In the following section we show the validity of this chain formation hypothesis by showing that the appearance of the second plateau, at lower conductance, can be controlled.

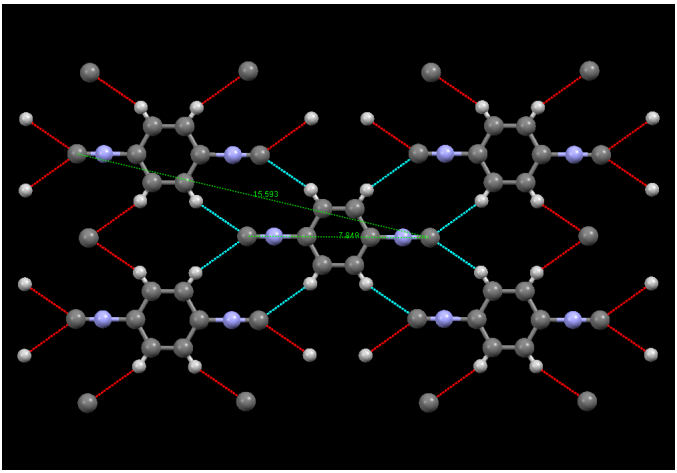

Figure 4.9.: Crystal structure of 1-NC as obtained by X-ray crystallography. The C-C length of one molecule is 7.849 Å, the length two molecules in series is 15.593 Å while three molecules in series measure 22.462 Å. The C-C distance of the neighbouring NC groups is 3.648 Å with a N-N distance of 4.030 Å.

4.2.1. Controlling the Chain Formation

If the lower conductance plateaus around G_2 are indeed formed by two molecules connected in series, the lower conductance plateaus should become rarer or even disappear if interactions between the molecules are impeded. A simple way to make the interactions less probable is to dilute the molecules. As the molecules will accumulate on the gold electrodes even at low concentrations, they were diluted both absolutely and also relatively by adding the monoisocyanide 1-mNC. Figure 4.10 shows conductance histograms from opening curves normalised to the number of curves. The data for the histograms was obtained from a single break junction over a period of 1 hour and 18 hours later (see inset). The solution first contained 0.25 µM of 1-NC and 2.5 µM of 1-mNC (black curve). The concentration of 1-mNC was increased to 25 µM for the later measurements (shown in red to magenta). The histogram counts are integrated over the intervals indicated in grey in order to quantify the size of histogram peaks. The

ranges of these intervals are obtained from figure 4.7 where they are shown as red lines. The inset of figure 4.10 shows these integrated counts relative to the counts from figure 4.7. The peaks around G_1 are similar to the one observed for pure 1-NC whereas the peaks around G_2 are less pronounced and vary in both amplitude and position. In the cyan and pink histograms no peak is observable below G_1. The cyan histogram, obtained after a waiting time of 18 hours, shows a larger value for the high conductance peak than the other histograms. After closing the junction strongly, the normal value for G_1 is restored (pink histogram). The progression of peak size is reflected in the inset of figure 4.10. The normalised counts for the high peak (light grey upward triangles) are high and stay constant except for the second to last outlier whereas the low peak counts (dark grey downward triangles) are lower for all histograms and slowly decrease over time. In figure 4.11a individual curves and a 2D histogram of the data corresponding to the pink histogram are shown. There are curves which show a clear plateau around G_1 (4 leftmost) and curves without plateaus. This translates to two bundles of curves in the 2D histogram. No plateaus were observed around G_2 or G_3. Some of the closing curves (b) show conductance jumps between G_2 and G_1 which is reflected by the low density in this conductance range of the 2D histogram (right). Figure 4.12 shows typical opening and closing curves of pure 1-mNC for comparison. No reproducible plateaus are observed.

1-mNC suppresses the conductance plateaus around G_2 to a varying degree when added to a dilute solution of 1-NC. This suppression is attributed to the formation of monolayers consisting of both molecules which lowers the probability of two 1-NC being close enough for interactions at the end of the G_1 plateau. To get the G_2 plateau to completely disappear, a waiting time on the order of 10 hours was necessary. This time could allow the molecules to rearrange on the metal surface. Also, isocyanides could oxidise to isocyanates due to residual oxygen in the solution which would further decrease the surface concentration of 1-NC [42]. The increase of the high conductance value after a long waiting time and its return to G_1 after strongly closing the junction is attributed to a blunting and resharpening of the electrode tips [27]. The fact that the lower conductance peaks can be suppressed by addition the monoisocyanide further supports the hypothesis of molecular chain formation.

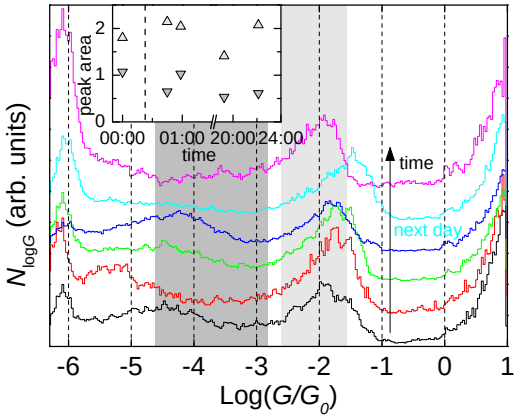

Figure 4.10.: Conductance histograms of mixed solutions with 1-NC 0.25 µM and 1-mNC 2.5 µM (black) and 25 µM (red to pink). Time increases from black to pink. The counts are normalized to the number of curves per histogram. The inset shows normalized histogram counts integrated over the ranges indicated in grey, also shown as red lines in figure 4.6. The peak size is shown relative to the peaks in figure 4.6. The dashed vertical line indicates the change in 1-mNC concentration.

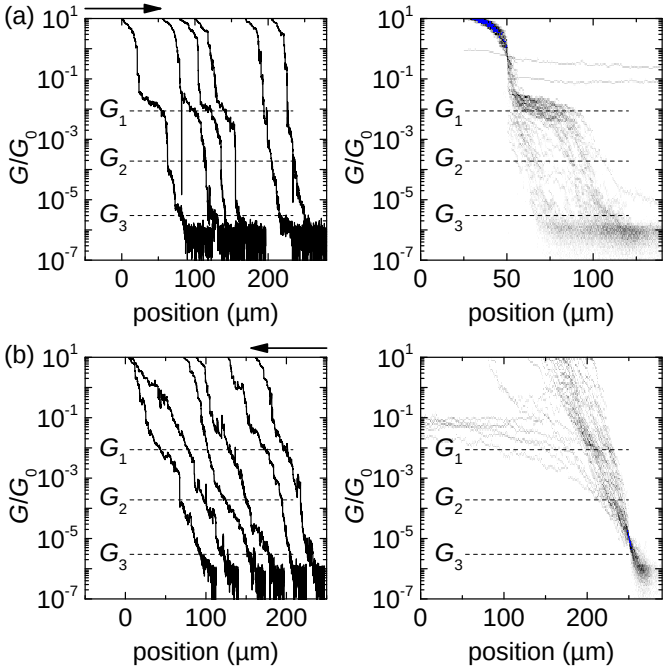

Figure 4.11.: (a) Typical opening curves of 1-NC 0.25 µM and 1-mNC 25 µM in THF/mesitylene 1:4 (left) and a 2D histogram of 50 consecutive opening curves (right). Plateaus are observed around $8.8 \cdot 10^{-3}\, G_0$. (b) Matching closing curves (left) and a 2D histogram of 50 consecutive closing curves aligned at $10^{-5}\, G_0$ (right). Jumps to the conductance value of the opening plateaus are observed in some which is reflected by the lower density around $1 \cdot 10^{-3}\, G_0$ in the 2D histogram (right).

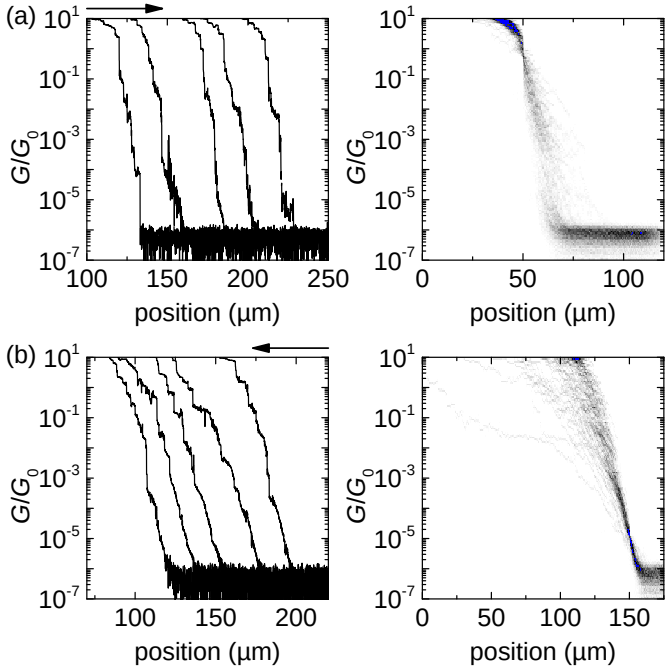

Figure 4.12.: (a) Typical opening curves of 1-mNC 0.25 mM in THF/mesitylene 1:4 (left) and a 2D histogram of 100 consecutive opening curves (right). The curves are noisy but no reproducible plateaus are observed. (b) Matching closing curves (left) and a 2D histogram of 100 consecutive closing curves aligned at $10^{-5}\,G_0$ (right). The curves show some irregularities and jumps around $10^{-3}\,G_0$ and close to $1\,G_0$ with an approximately exponential increase on average.

4.3. Systematic Comparison of Different Diisocyanide Molecules

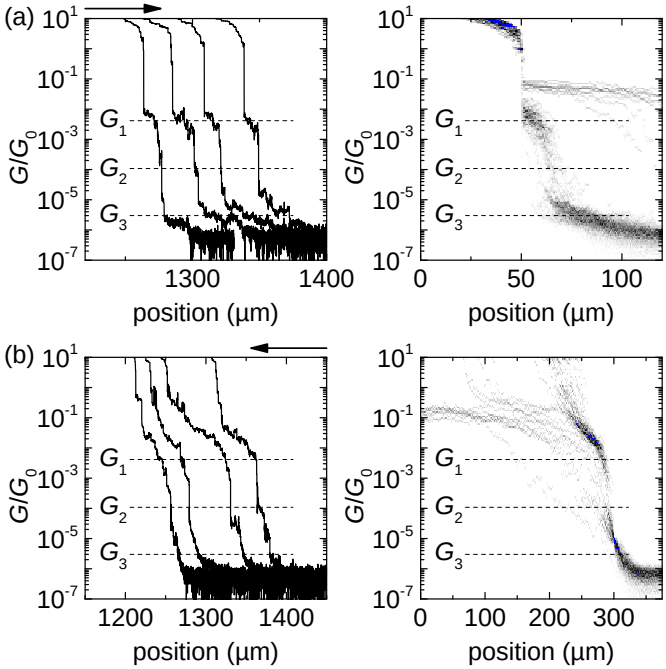

Figure 4.13.: (a) Typical opening curves of 2-NC 0.25 mM in THF/mesitylene 1:4 (left) and a 2D histogram of 43 consecutive opening curves (right). Plateaus are observed around $4.1 \cdot 10^{-3}\,G_0$. (b) Typical closing curves of 2-NC (left) and a 2D histogram of 43 consecutive closing curves aligned at $5 \cdot 10^{-5}\,G_0$. Jumps to molecular contacts are observed.

To determine the effect of molecular length on the conductance traces, 2-NC with a length between 1-NC and 3-NC was also measured. The results are shown in figure 4.13. Clear plateaus around $G_1 = 4.1 \cdot 10^{-3}\,G_0$ are observed in opening curves. A lower plateau is seen in single curves at $G_3 \approx 3 \cdot 10^{-6}\,G_0$ close to the background noise. In addition, very short plateaus are seen in about 50 % of the curves around $G_2 = 1.1 \cdot 10^{-4}\,G_0$ (see first two curves). The G_2 plateaus do not show in the 2D histogram due to the low number of counts. G_2 was obtained from a histogram of selected curves which show a plateau in this

range (figure 4.3, orange). In closing curves, jumps to approximately G_1 are observed.

Table 4.1 gives an overview of the conductance values and lengths of all molecules investigated in this chapter. The conductance values were obtained from histograms (figure 4.3) of opening curves for values larger than $10^{-5}\,G_0$ or estimated from single curves for lower values. The molecular lengths were estimated by optimizing structures in the software Avogadro[1] using the MMFF94s force field and from X-ray crystal structures in the case of 1-NC. In figure 4.14 conductance values of the isocyanide molecules are plotted against molecular length. An exponential decay function $G = G_A \exp(-\beta l)$ is fitted to the highest conductance G_1 of 1-NC, 2-NC and 3-NC and shown as black line. The data fits this exponential decay nicely with a decay constant of $\beta = 0.34\,\text{Å}^{-1}$ which is in agreement with typical literature values for conjugated molecules. See for example reference [7] and references therein. The green square labelled as 1-1 corresponds to G_2 of 1-NC and the length estimated for two molecules in series. The open green star next to the green square is plotted at the length obtained from the crystal structure. Both symbols are below the exponential decay line which is expected due to the additional tunnelling barrier between the molecules. The same is true for the even lower conductance value G_3 (shown as 1-1-1) estimated from single opening curves and the second conductance value of 2-NC (higher 2-2).

Molecule	Length of 1, 2, 3 (Å)	G_1 (G_0)	G_2 (G_0)	G_3 (G_0)
1-NC	7.876, 14.679, 21.484	$8.7 \cdot 10^{-3}$	$1.9 \cdot 10^{-4}$	$\approx 3 \cdot 10^{-6}$
X-ray data	7.849, 15.593, 22.462			
2-NC	10.064, 18.759, 27.525	$4.1 \cdot 10^{-3}$	$1.1 \cdot 10^{-4}$	$\approx 3 \cdot 10^{-6}$
3-NC	12.195, 23.288	$2.0 \cdot 10^{-3}$	$\approx 2 \cdot 10^{-6}$	
3-CN	12.311	$3.6 \cdot 10^{-5}$		
3-SAc	10.685	$1.4 \cdot 10^{-3}$		

Table 4.1.: Table of all molecules with two linker groups measured in this chapter. The molecular lengths are measured from the atoms expected to bind to the gold electrodes (C–C for isocyanides, N–N for the cyanide and S–S for the thiol) in structures obtained from Avogadro and X-ray crystallography. The conductance values were obtained from histograms of opening curves (figure 4.3).

It is not clear whether the short plateaus of 2-NC at G_2 really correspond to the 2-2 situation or whether they should be attributed to π–π stacking between the extended aromatic structure of naphthalene [7]. If the lower conductance G_3 should correspond to a chain of two molecules, the barrier between the

[1] http://avogadro.openmolecules.net/

molecules would have to be much larger than in the 1-NC case. G_3 is actually more likely to correspond to three molecules in series (2-2-2). For 3-NC, G_2 is also lower than expected for the 3-3 situation. Computational studies to estimate mechanical interactions and electronic coupling between molecules could help to answer this remaining questions and are in progress at the time of writing.

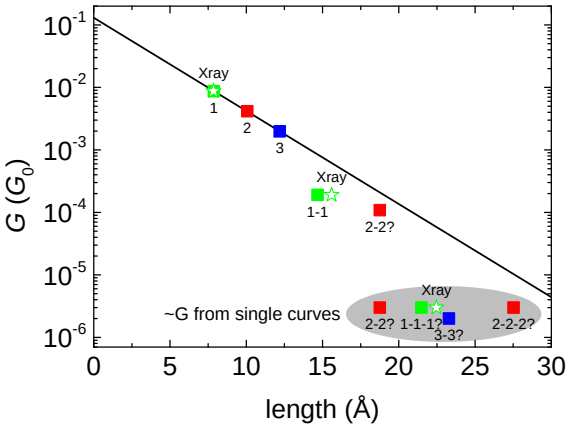

Figure 4.14.: Conductance values of the diisocyanide molecules against estimated lengths from the Avogadro program (solid squares) and lengths from X-ray structures (open stars). 1-NC in green, 2-NC in red, 3-NC in blue. The conductance values above $10^{-5}\,G_0$ were obtained from histograms of opening curves (figure 4.3) whereas the three lowest values indicated by the grey ellipse are estimated from single opening curves. An exponential decay fit to the highest conductance values of 1-NC, 2-NC and 3-NC is shown as a solid black line. Its decay constant is $\beta = 0.34\,\text{Å}^{-1}$. The assignment of some conductance values to molecular arrangements is tentative. Those uncertain points are indicated by question marks.

4.4. Conclusions

In a comparative study of biphenyl molecules with isocyanide, cyanide and thiol linker groups, biphenyl isocyanide (3-NC) was found to form molecular junctions most reliably and at the highest conductance value. The thiol compound (3-SAc) showed conductance plateaus with a lower probability but at a similar conductance value. The cyanide (3-CN) had a plateau yield similar to (3-NC) but at a lower conductance. The isocyanides (3-NC and also the shorter

2-NC and 2-NC) showed conductance jumps in closing curves with a very high probability. 1-NC reliably showed additional lower conductance values both in opening plateaus and between the closing jumps which can be suppressed by adding 1-mNC which contains only one isocyanide group. The high probability for isocyanides to jump to contact is attributed to their upright arrangement on the gold surface. The additional lower conductance plateaus are interpreted to correspond to chains of two or more molecules. The chaining is presumed to be caused by attractive interactions between molecules.

Isocyanides turned out to be an interesting linker group for the use in molecular junctions. They form junctions very reliably and show higher conductance values than thiols, pyridines or cyanides. Their tendency to jump to contact when closing and to form chains of molecules are particularly interesting. One could for example imagine a break junction experiment where two or more different molecular species are chained to obtain an asymmetric system. A possible application would be the connection of two self-assembled monolayers from different molecules which are both contacted by solid electrodes. Such a device can be imagined to work as a diode or solar cell.

Chapter 5

Additional Investigations

During the research work for this thesis, several molecules were investigated in addition to the main projects. Some interesting experimental results from these side projects are the topic of this chapter.

5.1. Further Linker Groups

Two linker groups were investigated in addition to the thiol and pyridine groups already discussed in the previous chapters. The amine group is successfully used in other groups with other setups but the plateau yield in our setup was very low so far. The following section summarizes the results from the amine measurements and lists possible reasons for the low amount of plateaus. The double thiol anchor group is an attempt to increase the mechanical stability of the molecule–metal bond.

5.1.1. Amines

Amines are well-studied linker groups for single molecular junctions. They are shown to reliably form molecular junctions to gold with well-defined conductance in both STM and MCBJ setups [29, 49, 53, 54]. Diaminooctane and OPE diamine were both measured in the MCBJ setup used in this work.

The solubility of diaminooctane was found to be weak in most of the tested solvents. This prevented the fabrication of a 1 mM solution as is commonly used [29, 49, 53, 54]. Dichloromethane was found to dissolve most of the molecule and was therefore used for the measurements. Figure 5.1 shows a measurement of diaminooctane. Typical opening curves are shown on top (first 4). Plateaus were observed very rarely. Only 5 out of the 200 opening curves analysed for this figure contained plateaus. These curves are shown as the last 5 curves in the top graph. On the left a histogram of all 200 opening curves is shown. 2.5 % of plateau yield is not enough to translate into a histogram peak. In the histogram from the 5 selected curves with plateaus (right) a clear peak is visible

at about $3.4 \cdot 10^{-5}\, G_0$. This conductance value is in approximate agreement with the work by by Hybertsen et al. [49].

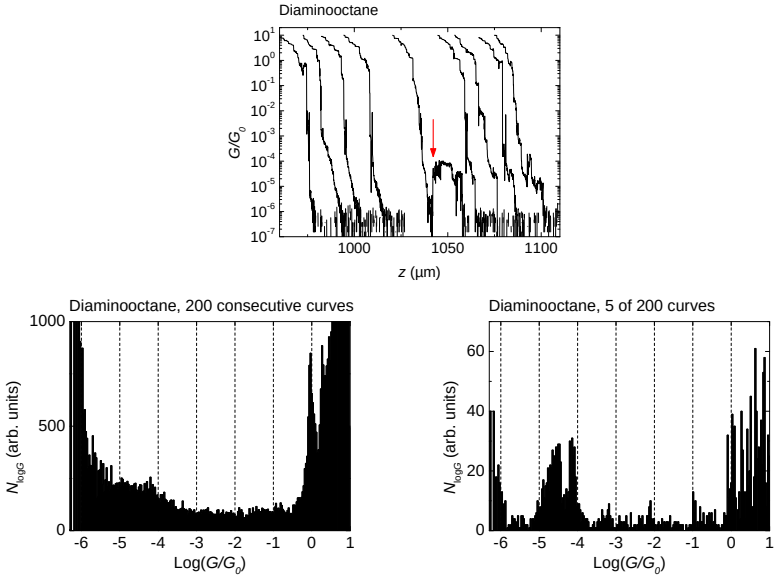

Figure 5.1.: Measurement of < 1 mM diaminooctane in dichloromethane. Top: Typical opening curves (first 4) and curves with plateaus (last 5). Left: Conductance histogram of 200 consecutive opening curves. No peak is observed. Right: Conductance histogram of the 5 out of 200 curves showing a plateau.

The plateau yield is slightly higher for OPE diamine. Figure 5.2 shows a measurement with a concentration of 0.25 mM in THF/mesitylene 1:4. In this case, the plateau yield is about 10 % which is still not enough to show as a peak in the histogram without data selection (left). Selecting curves with plateaus leads to a prominent peak in the histogram at about $3.7 \cdot 10^{-5}\, G_0$ (right).

Opening curves of both amine molecules show "broken plateaus" in some cases. Examples of such curves are indicated by red arrows in figures 5.1 and 5.2. In those curves the conductance decreases to a value below the detection limit before jumping back up to the plateau value.

In summary, both amine molecules investigated in this work show plateaus too infrequently to translate to histogram peaks without data selection. A possible reason for the low plateau yield is the different geometry of the MCBJ setup compared to STM setup (tip–tip vs. tip–plane). Another difference is the

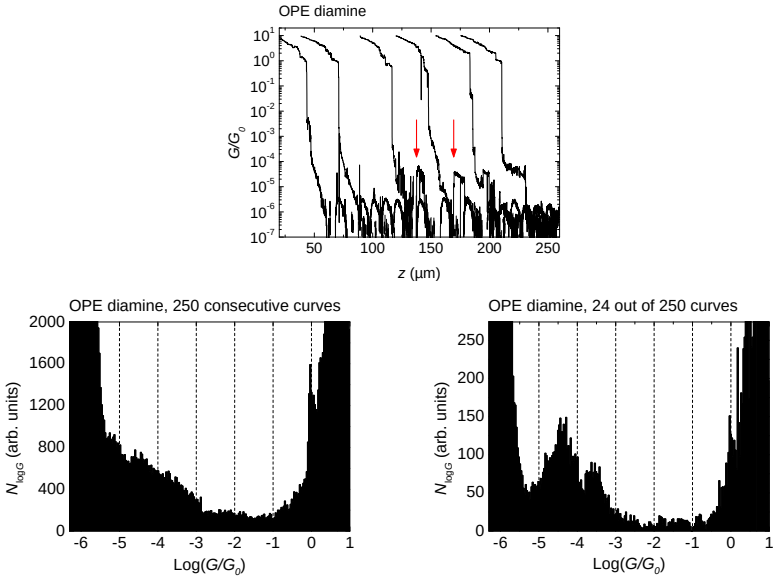

Figure 5.2.: Measurement of 0.25 mM OPE diamine in THF/mesitylene 1:4. Top: Typical opening curves without plateaus (first 2) and with plateaus (last 4). Left: Conductance histogram of 250 consecutive opening curves. No peak is observed. Right: Conductance histogram of the 24 out of 200 curves showing a plateau.

opening speed of the electrodes which is much slower in the present setup than in most STM break junction experiments. Finally, contaminations of the gold surface could impede the junction formation.

5.1.2. Double Thiol Anchor Group

Stable electrodes–molecule bonds are desirable for most experiments and possible applications with molecular junctions. The binding energy and stiffness of a single chemical bond to gold is fundamentally limited so other approaches are needed in order to gain substantially more stability. A possible way to increase the stability of molecular junctions is therefore to increase the number of bonds to the electrodes by adding additional binding groups to the molecule. SS-OPE-SS is a molecule designed according to this strategy. It is shown in figure 5.3. The molecule based on the normal S-OPE-S structure with the addition of two thiol groups in meta positions. Hexyl side groups are also added to compensate for the lower solubility due to the additional thiol groups.

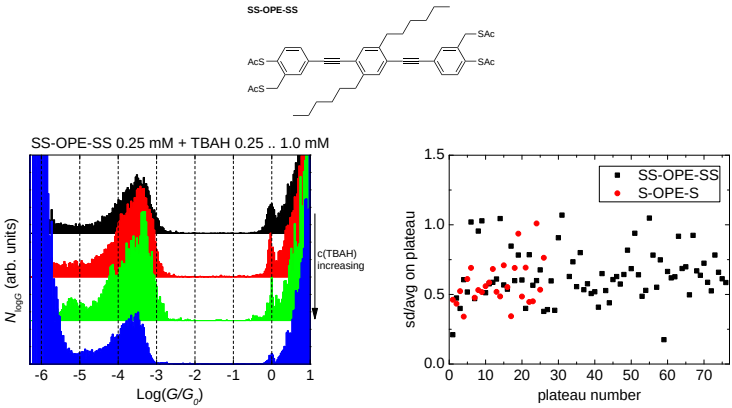

Figure 5.3.: Top: Molecular structure of SS-OPE-SS. Left: Measurement of 0.25 mM SS-OPE-SS in THF/mesitylene 1:4. Four conductance histograms of opening curves of the same sample. The concentration of TBAH increases from top to bottom from equimolar to SS-OPE-SS up to a 4:1 ratio. The histogram counts are normalised to the number of curves. Right: The standard deviations on conductance plateaus divided by the average conductance values of the plateaus of SS-OPE-SS compared to S-OPE-S.

In figure 5.3 normalised conductance histograms of opening curves with SS-OPE-SS are shown. The concentration of TBAH was increased from one equivalent of TBAH per SS-OPE-SS (black histogram) to a 4:1 ratio (blue). No significant change in peak position or shape is observed and the histograms match those of S-OPE-S (figure 1.4). The conductance variations on plateaus were analysed by calculating the standard deviation on a plateau normalised by its average conductance. A scatter plot of those normalized standard deviation values for both SS-OPE-SS and S-OPE-S is shown on the right. No significant difference is observed.

The similar conductance histograms for varying TBAH concentrations are to be expected for two reasons. First, if the molecule is bound to the gold electrodes with one thiol the second thiol is very close to the gold surface. Spontaneous bond formation is then very likely even with the acetyl group still attached. Second, the thiol groups connected in the meta position couple only weakly to the delocalised π system of the molecule and are additionally separated by a methyl group. The conductance increase by the two additional bonds could therefore be insignificant. The very similar conductance variations on plateaus of both SS-OPE-SS and S-OPE-S lead to the conclusion that the variations are not dominated by bond instability or that the second linker group does not bind to the electrodes. As S-OPE-S already forms stable plateaus, the

former seems more likely.

In conclusion, SS-OPE-SS forms molecular junctions reliably, very similar to the well-known S-OPE-S. No difference between the two molecules can be discerned in the low bias opening and closing cycles presented. An investigation of the long term stability of the molecular junctions as in chapter 2 could reveal differences between the molecules as could measurements at varying bias (chapter 3). Preliminary IV measurements hinted to a stronger non-linearity for SS-OPE-SS as compared to S-OPE-S (not shown) but further measurements are needed to assess the significance of this difference.

5.2. Redox-active Molecules

Break junction measurements in electrolytic environments require the leakage current from the macroscopic parts of the electrodes to be lower than the current through the molecular junction. Due to the small exposed surface area of the break junction samples used in this work, they are well-suited for such measurements if counter electrodes are added to sample structures and a suitable reference electrode is used. The molecule OPVFCcenter shown in figure 5.4 was successfully measured by Songmei Wu [28]. In these measurements, the conductance of the molecule could be altered by electrochemically oxidising and reducing the ferrocene moiety. In order to complement these electrochemical measurement, OPVFcside was planned to be measured in the same way. In OPVFcside, the ferrocene moiety is connected in a way such that transport through the molecule should not follow a trace across the ferrocene. Comparing the electrochemical response of both OPVFccenter and OPVFcside would provide insight on the mechanism of the electrochemical gating. Namely, a similar response of both compounds would confirm the proposed principle of conductance change by the opening of an additional molecular energy level by oxidation.

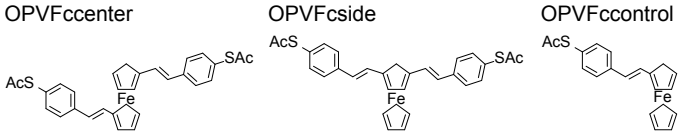

Figure 5.4.: Ferrocene-containing OPV compounds investigated in this section.

As the synthesis yield of OPVFcside was very low, only a few measurements could be performed. Figure 5.5 shows the most successful measurement with OPVFcside without electrochemical gating. Only about 10 % of the opening curves show plateaus which translates to a weak histogram peak. This plateau

yield was not high enough for electrochemical measurements. OPVFcside was measured with 4 different samples with the aim to reproduce Songmei Wu's measurements without electrochemical gating and to improve the plateau yield.

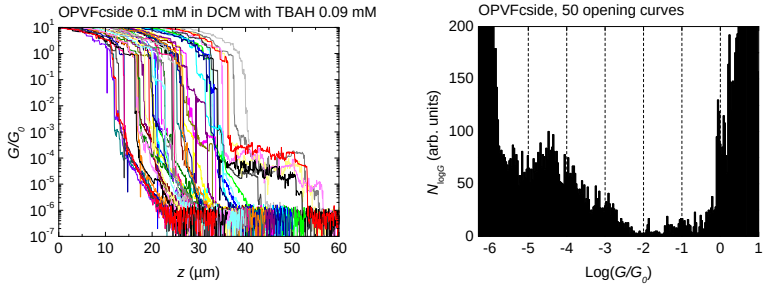

Figure 5.5.: Measurement of OPVFcside at a concentration of 0.09 mM in dichloromethane. Left: 50 consecutive opening curves. Only 6 of them show a clear plateau. Right: Histogram of the 50 opening curves. A weak peak at $3.7 \cdot 10^{-5}\, G_0$ is visible.

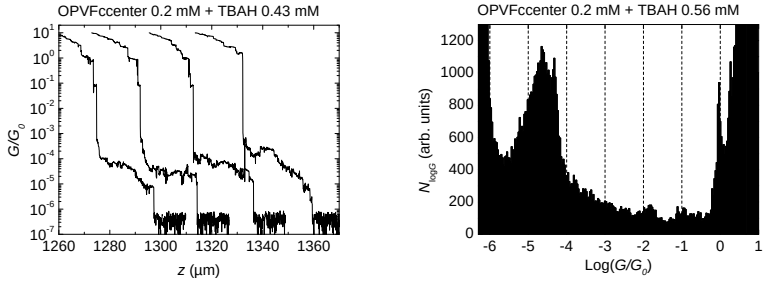

Figure 5.6.: Measurement of OPVFccenter at a concentration of 0.2 mM in THF/mesitylene 1:4 with an excess concentration of TBAH. Left: Typical opening curves. Right: Histogram of 250 consecutive opening curves. A prominent peak is found at $2.3 \cdot 10^{-5}\, G_0$.

It was found that a high concentration of TBAH of more than twice the molarity of the molecule is necessary to achieve a high plateau yield with OPVFccenter. Figure 5.6 shows typical opening curves which show clear plateaus. A histogram of 250 consecutive opening curves consequently features a prominent peak. It is not clear why a much higher concentration of TBAH was necessary than in the past measurements. The need for a high concentration of TBAH prevents electrochemical measurements as the TBAH ions contribute to leakage

current. Before attempting future break junction experiments with these molecules, the deprotecting problems have to be solved. Possibly, a lower concentration of both the molecular compound and of TBAH could work. Adding the whole amount of TBAH quickly in a single dose might also help as it lowers the chance for molecules with one remaining protection group to precipitate from the solution before reaching the junction. Alternatively, different reagents for deprotecting could be used [55].

Chapter 6

Summary and Outlook

The properties of molecular junctions have been investigated by the means of different transport experiments with mechanically controlled break junctions in liquid environments. First, the method of opening and closing cycles was introduced as a means to obtain conductance values of molecular junctions.

Then conductance fluctuations observed while not actively moving the electrodes were investigated. It was found that alkane dithiol molecules cause fluctuations of larger amplitude compared to measurements in pure solvent. These fluctuations are attributed to the binding and unbinding of molecules to the gold electrodes which demonstrates the limited lifetime of molecular junctions at room temperature.

To gain insight into molecular junctions beyond linear conductance measurements, a fast IV measurement method was developed which continuously records IV data at a rate of 100 curves/s. This allows for the observation of quick changes of the IV characteristics along single conductance plateaus. Both symmetric and asymmetric versions of OPE with different linker groups were measured and the data described by an analytic single level model. The coupling constant for the different molecule–metal bonds and the relative alignment of the dominant molecular energy level were obtained as fitting parameters of the model. It was found that transport through the symmetric molecules is dominated by different molecular orbitals depending on the linker group (HOMO vs. LUMO).

In a comparative study of biphenyl molecules with thiol, cyanide and isocyanide linker groups, isocyanide was found to form molecular junctions most reliably and at the highest conductance value. Additionally, the isocyanide molecules showed jumps to contact in most of the closing curves as opposed to the other investigated linker groups where such jumps are very rare. The most interesting observation with isocyanide molecules is the additional plateaus in opening curves at lower conductance values which are attributed to the chaining of two or more molecules.

Now that IV curves can be obtained at a high rates, it would be very interesting to measure 1-NC and the other isocyanide molecules with this method. The first question would be up to which bias voltage these junctions are stable. IV curves obtained along the lower plateaus could provide further evidence and insight on the proposed chain formation. Roughly, the voltage is expected to be divided equally between the two chained molecules so this chain IV curve should have a shape matching the middle half of the single molecule IV curve. The single level model might be extended to two levels and an additional coupling constant in between the molecules to model the measured data. Mixtures of different isocyanide molecules could be measured to observe chains consisting of different molecules. In addition, computational studies will hopefully prove useful for explaining if and how the molecules chain. Asymmetric molecules with different rectifying mechanisms are other interesting candidates for IV measurements as are tunable or switchable compounds, possibly relying on cross conjugation [56, 57]. For larger or even macroscopic devices, monolayers of isocyanide molecules could be formed on two separate surfaces and then connected.

If molecular electronics finally are to be incorporated into traditional semiconductor electronics, CMOS compatible processes have to be developed for the reliable formation of many molecular junctions. Possibly, metal wire or even silicon grids could be utilised to address a large number of junctions individually.

Bibliography

[1] A. I. Yanson, G. R. Bollinger, H. E. van den Brom, N. Agrait, and J. M. van Ruitenbeek, Nature **395**, 783 (1998).

[2] G. Rubio-Bollinger, S. R. Bahn, N. Agrait, K. W. Jacobsen, and S. Vieira, Physical Review Letters **87**, 026101 (2001).

[3] N. Agraït, A. L. Yeyati, and J. M. van Ruitenbeek, Physics Reports-Review Section Of Physics Letters **377**, 81 (2003).

[4] H. Ohnishi, Y. Kondo, and K. Takayanagi, Nature **395**, 780 (1998).

[5] M. T. González, S. M. Wu, R. Huber, S. J. van der Molen, C. Schönenberger, and M. Calame, Nano Letters **6**, 2238 (2006).

[6] R. Huber, M. T. González, S. Wu, M. Langer, S. Grunder, V. Horhoiu, M. Mayor, M. R. Bryce, C. S. Wang, R. Jitchati, C. Schönenberger, and M. Calame, Journal Of The American Chemical Society **130**, 1080 (2008).

[7] S. M. Wu, M. T. González, R. Huber, S. Grunder, M. Mayor, C. Schönenberger, and M. Calame, Nature Nanotechnology **3**, 569 (2008).

[8] Z. F. Huang, F. Chen, P. A. Bennett, and N. J. Tao, Journal Of The American Chemical Society **129**, 13225 (2007).

[9] M. Tsutsui, M. Taniguchi, and T. Kawai, Journal of the American Chemical Society **131**, 10552 (2009).

[10] W. Haiss, R. J. Nichols, H. van Zalinge, S. J. Higgins, D. Bethell, and D. J. Schiffrin, Physical Chemistry Chemical Physics **6**, 4330 (2004).

[11] R. J. Nichols, W. Haiss, S. J. Higgins, E. Leary, S. Martin, and D. Bethell, Physical Chemistry Chemical Physics **12**, 2801 (2010).

[12] M. Tsutsui, K. Shoji, K. Morimoto, M. Taniguchi, and T. Kawai, Applied Physics Letters **92**, 223110 (2008).

[13] M. Tsutsui, K. Shoji, M. Taniguchi, and T. Kawai, Nano Letters **8**, 345 (2008).

[14] X. G. Jiang, M. A. Dubson, and J. C. Garland, Physical Review B **42**, 5427 (1990).

[15] G. Jung, B. Savo, and Y. Yuzhelevski, Physical Review B **62**, 6674 (2000).

[16] R. T. Wakai and D. J. Vanharlingen, Applied Physics Letters **49**, 593 (1986).

[17] Y. Yuzhelevski, M. Yuzhelevski, and G. Jung, Review Of Scientific Instruments **71**, 1681 (2000).

[18] S. Machlup, Journal Of Applied Physics **25**, 341 (1954).

[19] B. Gotsmann, H. Riel, and E. Lortscher, Physical Review B **84**, 205408 (2011).

[20] L. Grüter, M. T. González, R. Huber, M. Calame, and C. Schönenberger, Small **1**, 1067 (2005).

[21] E. Leary, H. Hobenreich, S. J. Higgins, H. van Zalinge, W. Haiss, R. J. Nichols, C. M. Finch, I. Grace, C. J. Lambert, R. McGrath, and J. Smerdon, Physical Review Letters **102**, 086801 (2009).

[22] M. Paulsson, C. Krag, T. Frederiksen, and M. Brandbyge, Nano Letters **9**, 117 (2009).

[23] C. Li, I. Pobelov, T. Wandlowski, A. Bagrets, A. Arnold, and F. Evers, Journal Of The American Chemical Society **130**, 318 (2008).

[24] D. R. Jones and A. Troisi, Journal Of Physical Chemistry C **111**, 14567 (2007).

[25] J. Klafter and M. F. Shlesinger, Proceedings Of The National Academy Of Sciences Of The United States Of America **83**, 848 (1986).

[26] S. Boussaad, B. Q. Xu, L. A. Nagahara, I. Amlani, W. Schmickler, R. Tsui, and N. J. Tao, Journal Of Chemical Physics **118**, 8891 (2003).

[27] M. T. González, J. Brunner, R. Huber, S. M. Wu, C. Schönenberger, and M. Calame, New Journal Of Physics **10**, 065018 (2008).

[28] S. Wu, *Electrical conductance of single conjugated oligomers*, Ph.D. thesis, University of Basel (2009).

[29] J. R. Widawsky, M. Kamenetska, J. Klare, C. Nuckolls, M. L. Steigerwald, M. S. Hybertsen, and L. Venkataraman, Nanotechnology **20**, 434009 (2009).

[30] S. Y. Guo, J. Hihath, I. Diez-Perez, and N. J. Tao, Journal of the American Chemical Society **133**, 19189 (2011).

[31] W. J. Hong, D. Z. Manrique, P. Moreno-Garcia, M. Gulcur, A. Mishchenko, C. J. Lambert, M. R. Bryce, and T. Wandlowski, Journal of the American Chemical Society **134**, 2292 (2012).

[32] J. G. Simmons, Journal of Applied Physics **34**, 1793 (1963).

[33] J. M. Beebe, B. Kim, C. D. Frisbie, and J. G. Kushmerick, Acs Nano **2**, 827 (2008).

[34] M. L. Trouwborst, C. A. Martin, R. H. M. Smit, C. M. Guedon, T. A. Baart, S. J. van der Molen, and J. M. van Ruitenbeek, Nano Letters **11**, 614 (2011).

[35] E. H. Huisman, C. M. Guedon, B. J. van Wees, and S. J. van der Molen, Nano Letters **9**, 3909 (2009).

[36] S. Datta, Nanotechnology **15**, S433 (2004).

[37] L. Grüter, F. Y. Cheng, T. T. Heikkila, M. T. González, F. O. Diederich, C. Schönenberger, and M. Calame, Nanotechnology **16**, 2143 (2005).

[38] L. A. Zotti, T. Kirchner, J. C. Cuevas, F. Pauly, T. Huhn, E. Scheer, and A. Erbe, Small **6**, 1529 (2010).

[39] J. Cuevas and E. Scheer, *Molecular Electronics: An Introduction to Theory and Experiment (Nanotechnology and Nanoscience) (World Scientific Series in Nanotechnology and Nanoscience)* (World Scientific Publishing Company, 2010) pp. –.

[40] A. Tan, J. Balachandran, S. Sadat, V. Gavini, B. D. Dunietz, S. Y. Jang, and P. Reddy, Journal of the American Chemical Society **133**, 8838 (2011).

[41] J. R. Widawsky, P. Darancet, J. B. Neaton, and L. Venkataraman, Nano Letters **12**, 354 (2012).

[42] J. J. Stapleton, T. A. Daniel, S. Uppili, O. M. Cabarcos, J. Naciri, R. Shashidhar, and D. L. Allara, Langmuir **21**, 11061 (2005).

[43] R. Ramozzi, N. Cheron, B. Braida, P. C. Hiberty, and P. Fleurat-Lessard, New J. Chem. **36**, 1137 (2012).

[44] C. D. Zangmeister, S. W. Robey, R. D. van Zee, J. G. Kushmerick, J. Naciri, Y. Yao, J. M. Tour, B. Varughese, B. Xu, and J. E. Reutt-Robey, Journal of Physical Chemistry B **110**, 17138 (2006).

[45] M. Kiguchi, S. Miura, K. Hara, M. Sawamura, and K. Murakoshi, Applied Physics Letters **89**, 213104 (2006).

[46] E. Lörtscher, C. J. Cho, M. Mayor, M. Tschudy, C. Rettner, and H. Riel, Chemphyschem **12**, 1677 (2011).

[47] S. Hong, R. Reifenberger, W. Tian, S. Datta, J. I. Henderson, and C. P. Kubiak, Superlattices and Microstructures **28**, 289 (2000).

[48] J. Chen, L. C. Calvet, M. A. Reed, D. W. Carr, D. S. Grubisha, and D. W. Bennett, Chemical Physics Letters **313**, 741 (1999).

[49] M. S. Hybertsen, L. Venkataraman, J. E. Klare, A. CWhalley, M. L. Steigerwald, and C. Nuckolls, Journal Of Physics-Condensed Matter **20**, 374115 (2008).

[50] K. Horiguchi, S. Kurokawa, and A. Sakai, Journal Of Chemical Physics **131**, 104703 (2009).

[51] A. Mishchenko, D. Vonlanthen, V. Meded, M. Buumlrkle, C. Li, I. V. Pobelov, A. Bagrets, J. K. Viljas, F. Pauly, F. Evers, M. Mayor, and T. Wandlowski, ACS Nano Letters **10**, 156 (2010).

[52] I. Alkorta, I. Rozas, and J. Elguero, Theoretical Chemistry Accounts **99**, 116 (1998).

[53] L. Venkataraman, J. E. Klare, I. W. Tam, C. Nuckolls, M. S. Hybertsen, and M. L. Steigerwald, Nano Letters **6**, 458 (2006).

[54] Y. Kim, T. J. Hellmuth, M. Burkle, F. Pauly, and E. Scheer, Acs Nano **5**, 4104 (2011).

[55] H. Valkenier, E. H. Huisman, P. A. van Hal, D. M. de Leeuw, R. C. Chiechi, and J. C. Hummelen, Journal of the American Chemical Society **133**, 4930 (2011).

[56] G. C. Solomon, D. Q. Andrews, R. H. Goldsmith, T. Hansen, M. R. Wasielewski, R. P. Van Duyne, and M. A. Ratner, Journal of the American Chemical Society **130**, 17301 (2008).

[57] A. B. Ricks, G. C. Solomon, M. T. Colvin, A. M. Scott, K. Chen, M. A. Ratner, and M. R. Wasielewski, Journal of the American Chemical Society **132**, 15427 (2010).

[58] E. H. Huisman, M. L. Trouwborst, F. L. Bakker, B. de Boer, B. J. van Wees, and S. J. van der Molen, Nano Letters **8**, 3381 (2008).

Appendix A

Investigation of Other Molecules

A.1. Crown Ether molecule

A crown ether molecule (structure in figure A.1) was measured in an attempt to sense lithium ions. The molecule was suspected to undergo a conformational change after binding a lithium ion which should have an influence on the conductance. Two typical histograms of opening curves measured both with and without lithium bromide are shown in figure A.2. The molecule formed junctions very reliably which results in pronounced peaks in the histograms. The goal of sensing ions was not met, however, as no significant difference between the two histograms can be discerned. The lack of effect of the lithium salt was verified with more measurements and higher ion concentration.

In a discussion with David Vonlanthen, who synthesised the molecule, it was found that the affinity of lithium ions to the molecule was not high enough to overcome their affinity to THF. In future measurements, using a less polar solvent increase the affinity enough to enable ion sensing.

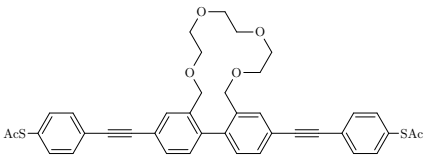

Figure A.1.: Structure of the crown ether molecule.

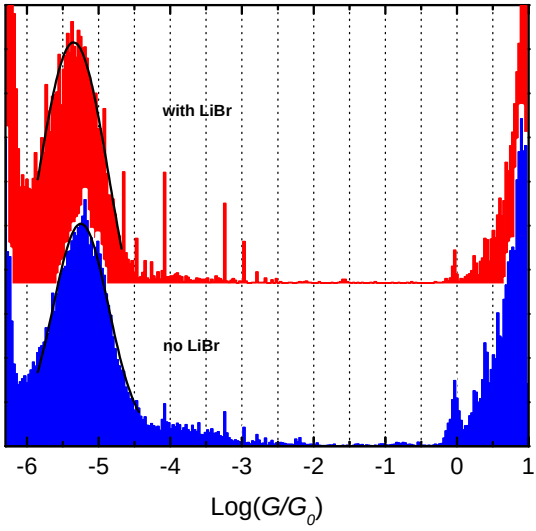

Figure A.2.: Histograms of opening curves measured with 0.25 mM solutions of the crown ether molecule in THF/mesitylene 1:4 with LiBr concentrations of 0 (bottom) and 3.33 mM. Both histograms show identical peak positions.

A.2. Br-OPE-Br, I-OPE-I

Bromine and iodine were investigated as possible linker groups. They have a lone electron pair that could interact with gold. Pure bromine and iodine are both known to dissolve gold. Figure A.3 shows the molecular structures of Br-OPE-Br and I-OPE-I that are investigated in this section. The iodine compound has two hexyl side groups attached to the central phenyl ring to increase solubility. For the bromine compound this was not found to be necessary.

Br-OPE-Br was measured at a concentration of 0.25 mM in both ethyl benzoate (figure A.4) and THF/mesitylene 1:4 (figure A.5). Both figures show a histogram of opening curves measured with pure solvent on the left. The data shown on the right was obtained with the same sample but with the solution replaced to contain the molecule. A clear peak cannot be identified with either solvent but there is a broad shoulder between 10^{-5} and $10^{-4}\,G_0$ in both cases. This shoulder does not show in the pure solvent histograms.

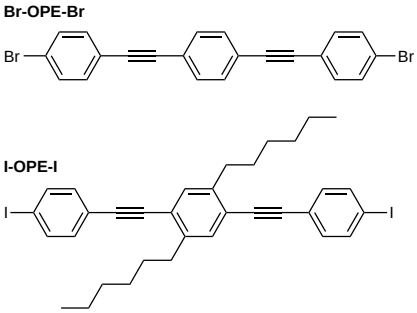

Figure A.3.: Structures of the Br-OPE-Br and I-OPE-I molecules.

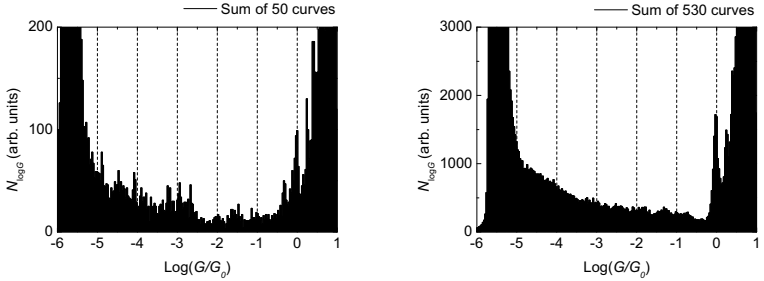

Figure A.4.: Histograms of opening curves measured in pure ethyl benzoate (left) and in a 0.25 mM solution of Br-OPE-Br in ethyl benzoate (right).

I-OPE-I was measured at a concentration slightly lower than 0.25 mM as the compound did not fully dissolve. Figure A.6 shows a measurement of pure solvent on the left. The histogram on the right was obtained after changing to the molecular solution. I-OPE-I was not found to show clear plateaus and histogram peaks in opening curves but it was found to suppress the $1\,G_0$ plateaus very efficiently. This effect is in direct contrast to the known stabilising effect of alkane dithiols on the atomic contact [58].

In summary, both Br-OPE-Br and I-OPE-I were measured to find out whether bromine and iodine are suitable as linker groups for molecular electronics. The bromine compound was shown to have very little effect on the opening curves. It might change the slopes slightly to cause a weak shoulder in the histograms between between 10^{-5} and $10^{-4}\,G_0$ but does not seem to form stable molecular junctions. I-OPE-I also does not seem to form molecular junctions but it does suppress the $1\,G_0$ plateaus. The mechanism of the gold plateau suppression

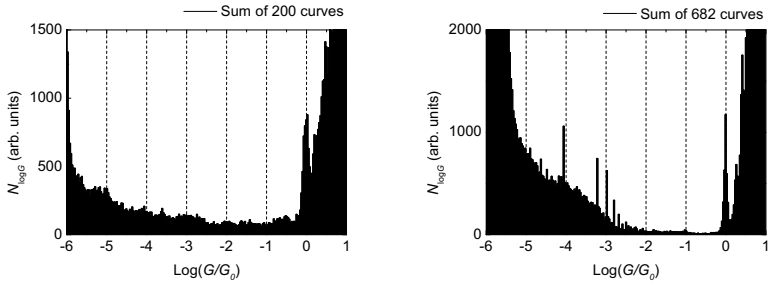

Figure A.5.: Histograms of opening curves measured in THF/mesitylene 1:4 (left) and in a 0.25 mM solution of Br-OPE-Br in THF/mesitylene 1:4 (right).

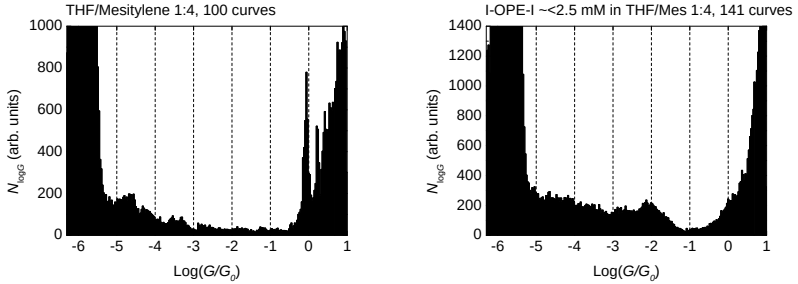

Figure A.6.: Histograms of opening curves measured in THF/mesitylene 1:4 (left) and in a < 0.25 mM solution of I-OPE-I in THF/mesitylene 1:4 (right). No clear molecular peaks are observed but the $1\,G_0$ peak has disappeared.

is not known. Possibly, the iodine compound or free iodine binds to gold atoms in a way which lowers either the stability of the monoatomic junctions or prevents their formation. It can be concluded that although both Br-OPE-Br and I-OPE-I seem to interact with the gold electrodes, neither bromine nor iodine are usable linker groups.

Appendix B

Specifications of IV converter

B.1. IV Converters

SP895/SP895a

The autoranging IV converter consists of the actual amplifier SP895 and the autoranging unit SP895a. Both units are housed in separate well-shielded aluminium boxes and coupled optically to prevent crosstalk from the autoranging unit to the amplifier. The available gain settings are 10^5 V/A, 10^6 V/A, 10^7 V/A and 10^8 V/A with input current noise densities of 408 fA/$\sqrt{\text{Hz}}$, 129 fA/$\sqrt{\text{Hz}}$, 41 fA/$\sqrt{\text{Hz}}$ and 13 fA/$\sqrt{\text{Hz}}$, respectively. The noise level is slightly higher with the switching spike killer commonly used to protect the sample from current spikes. The bandwidth is 800 Hz for the highest gain and 10 kHz for the other gain settings. The gain can either be automatically selected or set by hand.

SP895c/d

This IV converter is similar to the SP895/SP895a but offers a higher range of gain settings, namely 10^4 V/A (10 kHz), $0.47 \cdot 10^6$ V/A (10 kHz), $0.22 \cdot 10^8$ V/A (4 kHz) and 10^9 V/A (1 kHz) with input current noise densities of 1.5 pA/$\sqrt{\text{Hz}}$, 184 fA/$\sqrt{\text{Hz}}$, 33 fA/$\sqrt{\text{Hz}}$ and 5.3 fA/$\sqrt{\text{Hz}}$, respectively.

B.2. Effects of Large Ramp Speed on IV Converter Gain

When the conductance of the sample is high during IV measurements, the IV converter is driven into overload. The output voltage of the IV converter (operational amplifier) is limited to ± 10 V and will be truncated if it would have to reach higher or lower values to follow the shape of the input current.

This truncation increases the effective frequency of the signal which slightly lowers the open-loop gain of the operational amplifier. This in turn leads to an increase of the effective input resistance of the IV converter (R_{in} = [gain of IV converter]/[gain of OPA]).

The change in input resistance ΔR_{in} is found to depend linearly on the output ramp speed of the amplifier $\dot{V}_{\mathrm{out}}$ as shown in equation B.1. V_{window} is the range of the bias voltage allowed with the output voltage still in the allowed range and F_{IV} an amplifier-dependant constant.

Both $\dot{V}_{\mathrm{out}}$ and V_{window} can be defined in terms of system parameters (equations B.2 and B.3). V_{ramp} and f_{ramp} are the amplitude and the frequency of the voltage ramp, respectively, G_{amp} the gain of the IV converter, R_{sample} and R_{s} the sample and series resistance and m_{IV} the slope of the measured IV curve before saturation.

$$\Delta R_{\mathrm{in}} = F_{\mathrm{IV}} \cdot \dot{V}_{\mathrm{out}} / V_{\mathrm{window}} \tag{B.1}$$

$$\dot{V}_{\mathrm{out}} = V_{\mathrm{ramp}} \cdot 2 \cdot 2 \cdot f_{\mathrm{ramp}} / \underbrace{(R_{\mathrm{sample}} + R_{\mathrm{s}})}_{\approx 1/m_{\mathrm{IV}}} \cdot G_{\mathrm{amp}} \tag{B.2}$$

$$V_{\mathrm{window}} = 2 \cdot \frac{10\,\mathrm{V}}{m_{\mathrm{IV}} \cdot G_{\mathrm{amp}}} \tag{B.3}$$

Finally, we obtain an expression for the change in series resistance (equation B.4). $F_{\mathrm{IV}} \approx 0.012\,\Omega/\mathrm{Hz}$ has been determined from a set of measurements with different $\dot{V}_{\mathrm{out}}$. Although the change in input resistance is small relative to typical molecular conductance values, it is comparable to the sample resistance for closed junctions ($G \geq 1\,G_0$) and is therefore taken into account for the calculation of conductance values. At low conductance values, this correction is negligible as $\Delta R_{\mathrm{in}} \propto m_{\mathrm{IV}}^2 \propto G^2$.

$$\Delta R_{\mathrm{in}} = F_{\mathrm{IV}} \cdot 4 \cdot V_{\mathrm{ramp}} \cdot f_{\mathrm{ramp}} m_{\mathrm{IV}}^2 G_{\mathrm{amp}}^2 / 20\,\mathrm{V} \tag{B.4}$$

Appendix C

Additional IV Investigations

C.1. Effect of Temperature on Single Energy Level Model

Finite temperature can be included in the single level model by evaluating equation 3.7 numerically. This has been done to investigate the effect of temperature in the model. Fits to a typical N-OPE-N measurement are shown in figure C.1 and the corresponding fit parameters are given in table C.1. The effect of temperature on both the shape of the fitted curve and the obtained parameters is negligible at room temperature. For higher temperatures, all fit parameters increase.

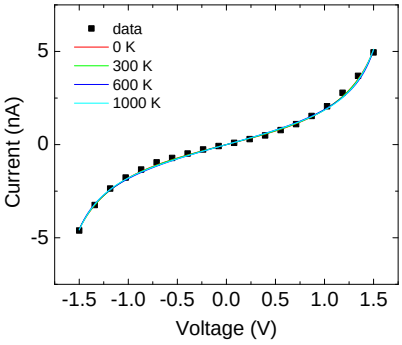

Figure C.1.: Typical IV curve of N-OPE-N at a low conductance value shown at reduced resolution (black squares). Fits of the single level model at different assumed temperatures are shown in red (0 K), green (300 K), blue (600 K) and cyan (1000 K).

T	0 K	300 K	600 K	1000 K
E_0 (eV)	0.99	1.01	1.14	1.34
Γ_1 (meV)	2.04	2.10	2.43	2.83
Γ_2 (meV)	2.10	2.16	2.49	2.91

Table C.1.: Fit parameters obtained for different assumed temperatures. Fits shown in figure C.1

C.2. Effect of Bias Range

Table C.2 shows fitting parameters obtained from a typical IV curve of N-OPE-N with different bias ranges used for the fit. There is a clear trend for the parameters to decrease for a reduced fit range. For this reason, the same bias range was used for all the data used in comparisons.

fit range	± 1.5 V	± 1.25 V	± 1.0 V
E_0 (eV)	0.99	0.91	0.82
Γ_1 (meV)	2.03	1.77	1.55
Γ_2 (meV)	2.12	1.89	1.70

Table C.2.: Fit parameters obtained for different bias ranges.

C.3. Unreasonable Fit Parameters

Noise or sudden jumps in the IV curves are then likely to give rise to unreasonable fitting parameters in asymmetric IV curves ($\Gamma_{\text{high}} \approx 0.5\,\text{eV}$ and $\Gamma_{\text{low}} \approx 5 \cdot 10^{-5}\,\text{eV}$). Such outlying parameters lead to an IV curve that is similar to one obtained with reasonable coupling constants so low noise data is necessary to prevent unrealistic fitting parameters. Figure C.2 shows two IV curves from N-OPE-S obtained right after each other without any averaging. The fit works well in (a) whereas a small current jump in (b) leads to unreasonable coupling constants.

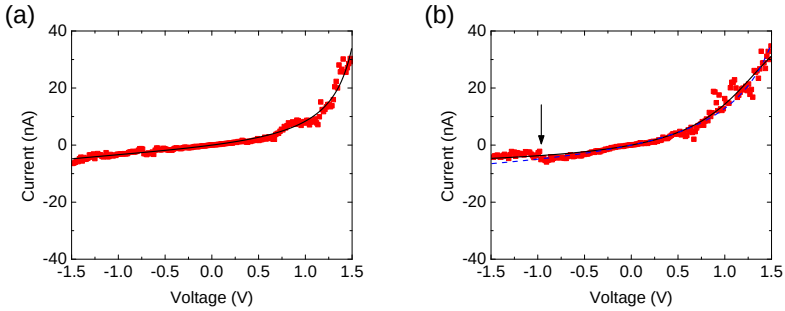

Figure C.2.: IV data obtained from consecutive single voltage ramps in N-OPE-S shown as red squares and single level model fits as solid black lines. (a) Reasonable fit parameters are obtained: $E_0 = 1.3\,\text{eV}$, $\Gamma_1 = 2.82\,\text{meV}$, $\Gamma_2 = 8.55\,\text{meV}$. (b) A small jump in the current data (indicated by arrow) leads to unreasonable fit parameters: $E_0 = 1.3\,\text{eV}$, $\Gamma_1 = 6.87 \cdot 10^{-5}\,\text{eV}$, $\Gamma_2 = 0.59\,\text{eV}$. When Γ_1 is fixed to the value obtained in (a), the fit leads to reasonable parameters while the fitted function looks only slightly different (shown as blue dashed line).

Appendix D

Supplementary Information for Fluctuations Chapter

D.1. Derivation of the distribution of lifetimes

Let $p(t)dt$ be the probability for no decay before time t (which we call $A(t)$) followed by a decay between times t and $t+dt$ (which is $1/\tau \cdot dt$). The probability density of the lifetimes is then $p(t) = A(t)/\tau$.

The probability for no decay until time $t + dt$ is

$$A(t + dt) = A(t)\left(1 - \frac{dt}{\tau}\right) \tag{D.1}$$

which we can rearrange to

$$\frac{A(t + dt) - A(t)}{dt} = \frac{dA(t)}{dt} = -\frac{A(t)}{\tau} \tag{D.2}$$

The solution of this differential equation is

$$A(t) = \exp\left(\frac{-t}{\tau}\right) \tag{D.3}$$

The probability density is then

$$\Rightarrow p(t) = A(t)/\tau = \frac{1}{\tau}\exp\left(\frac{-t}{\tau}\right) \tag{D.4}$$

Curriculum Vitae

Jan Gerhard Brunner
July 23 1981 born in Basel BS

Education

1997–2000	Gymnasium Oberwil (C Typus)
2001–2003	Physics Basic Course (ETHZ)
2003–2006	Bachelor of Science in Nanosciences at the University of Basel
2006–2008	Master of Science in Nanosciences at the University of Basel Master Thesis in the group of Prof. C. Schönenberger: "Conductance Fluctuations in Molecular Junctions"
2008–2012	PhD in Nanosciences at the University of Basel PhD Thesis in the group of Prof. C. Schönenberger under the supervision of M. Calame

Publications

Publications

- *Conductance values of alkanedithiol molecular junctions*, M. T. González, J. Brunner, R. Huber, S. Wu, C. Schönenberger and M. Calame
  New J Phys **10**, 065018 (2008)

- *Signal-to-noise ratio in dual-gated silicon nanoribbon field-effect sensors*, A. Tarasov, W. Fu, O. Knopfmacher, J. Brunner, M. Calame and C. Schönenberger
  Appl. Phys. Lett. **98**, 012114 (2011)

- *Force–conductance correlation in individual molecular junctions*, C. Nef, P. L. T. M. Frederix, J. Brunner, C. Schönenberger and M. Calame
  Nanotechnology **23**, 365201 (2012)

- *Two-Level Conductance Fluctuations in Molecular Junctions*, J. Brunner, M. T. González, C. Schönenberger and M. Calame
  (to be submitted)

- *Investigation of Symmetry Aspects in Molecular Junctions by IV Spectroscopy*, J. Brunner, S. Grunder, C. Schönenberger, M. Mayor and M. Calame
  (in preparation)

- *Isocyanide Anchor Groups in Molecular Electronics*, J. Brunner, M. Gantenbein, C. Schönenberger, M. Mayor and M. Calame
  (in preparation)

Oral Presentations

- *Conductance Fluctuations in Molecular Junctions*, J. Brunner, S. Wu, R. Huber, M. T. González, S. Grunder, M. Mayor, C. Schönenberger and

M. Calame
Talk at the Molecular Electronics Workshop, University of Bern, May 12, 2009

- *Conductance Fluctuations in Molecular Junctions*, J. Brunner, S. Wu, R. Huber, M. T. González, S. Grunder, M. Mayor, C. Schönenberger and M. Calame
Talk at the SNI workshop, EMPA Dübendorf, June 24, 2011

Poster Contributions

- *Conductance Fluctuations in Molecular Junctions*, J. Brunner, S. Wu, R. Huber, M. T. González, M. Mayor, C. Schönenberger and M. Calame
Poster at the Trends in Nanoscience Symposium 2009, Irsee, February 28-March 4, 2009

- *Conductance Fluctuations in Molecular Junctions*, J. Brunner, S. Wu, R. Huber, M. T. González, M. Mayor, C. Schönenberger and M. Calame
Poster at the SwissNano 2009, Basel, June 11-12, 2009

- *Conductance Fluctuations in Molecular Junctions*, J. Brunner, S. Wu, R. Huber, M. T. González, M. Mayor, C. Schönenberger and M. Calame
Poster at the International Conference on Molecular Electronics 2010, Emmetten, January 5-9, 2010

- *Conductance Fluctuations in Molecular Junctions*, J. Brunner, S. Wu, R. Huber, M. T. González, M. Mayor, C. Schönenberger and M. Calame
Poster at the SPS meeting 2010, Basel, June 21-22, 2010

- *Investigation of Symmetry Aspects in Molecular Junctions by IV Spectroscopy*, J. Brunner, S. Grunder, C. Schönenberger and M. Calame
Poster at the Workshop Future Directions of Molecular Electronics, Leiden, June 25-29, 2012

Acknowledgements

I want to thank Christian Schönenberger and Michel Calame for giving me the opportunity to do my PhD in this group. A special thank goes to my advisor Michel for invaluable feedback, guiding and motivation.

I have learnt a lot about molecular electronics and break junctions from Teresa González, Roman Huber and Songmei Wu. My project student Andreas Wepf performed preliminary IV measurements which helped to develop the new and improved measurement technique. Whenever I had technical problems or questions, Heinz Breitenstein and Silvester Jakob from the mechanical workshop or Michael Steinacher, Werner Erni and Sascha Linder from the electronics lab were very helpful. For administrative matters Audrey Fischer, Astrid Kalt and Barbara Kammermann provided services whenever needed.

My colleagues Cornelia Nef, Toni Fröhlich, Jon Agustsson, Claire Barrett and Zheng-Ming Wu who work or worked on related projects were always responsive to my questions and sometimes also posed challenging and inspiring questions to me. The chemists of Marcel Mayor's group, especially Sergio Grunder, David Vonlanthen, Nicolas Jenny and Markus Gantenbein provided most of the molecules used in the experiments and were also available for chemistry-related questions.

The nanowire sensor team consisting of Oren Knopfmacher, Alexey Tarasov, Mathias Wipf and Ralph Stoop was an entertaining company in the office.

I would also like to thank the rest of the group. It was nice to work and go on group excursions with Veronica Savu, Andreas Baumgartner, Wangyang Fu, Romain Maurand, Markus Weiss, Matthias Bräuninger, Samuel d'Hollosy, Gabor Fabian, Frank Freitag, Jörg Gramich, Thomas Hasler, Stefan Nau, Peter Rickhaus, Julia Samm, Jens Schindele, Neeraj Adsul, Samuel Vogel, Kristine Bedner, Hagen Aurich, Szabolcs Csonka, Alex Eichler, Lukas Hofstetter, Haichao Huang, Dino Keller, Andreas Kleine, Jianhui Liao and Sense Jan van der Molen.

In addition I would like to thank my family for supporting me during my studies.

Finally, I want to thank Nicolás Agraït and Paolo Samorì for reading my thesis and for joining the defence committee.